mathematics

MDPI

Article

Modern Dimensional Analysis-Based Heat Transfer Analysis: Normalized Heat Transfer Curves

Ioan Száva [1,*], Sorin Vlase [1,2,*], Ildikó-Renáta Száva [1], Gábor Turzó [3], Violeta Mihaela Munteanu [1], Teofil Gălățanu [1], Zsolt Asztalos [1] and Botond-Pál Gálfi [1]

[1] Department of Mechanical Engineering, Transylvania University of Brasov, B-dul Eroilor 29, 500036 Brasov, Romania
[2] Romanian Academy of Technical Sciences, B-dul Dacia 26, 030167 Bucharest, Romania
[3] Veiki Energia, Research and Design in Heat-Technology Co., Ltd., 30923 Budapest, Hungary
* Correspondence: eet@unitbv.ro (I.S.); svlase@unitbv.ro (S.V.)

Abstract: In this contribution, the authors continued their initial study on the efficiency of the analysis of experimentally obtained temperature curves, in order to determine some basic parameters that are as simple and reliable as possible, such as "*m*", the heat transfer coefficient. After the brief review of the previous results, on which the present article is based, the authors offered a brief argumentation of the importance of dimensional methods, especially the one called modern dimensional analysis, in these theoretical-experimental investigations regarding the propagation of the thermal field of structural elements with solid sections, and especially with tubular-rectangular sections. It could be concluded that modern experimental investigations mostly follow the behavior of models attached to the initial structures, i.e., prototypes, because there are clear advantages in this process of forecasting the behavior of the prototype based on the measurement results obtained on the attached model.

Keywords: experimentally obtained temperature distribution law; relative temperature curves; *m* parameter's variation laws; 2D steel structural elements; testing bench; reduced-scale models

MSC: 74S05

Citation: Száva, I.; Vlase, S.; Száva, I.-R.; Turzó, G.; Munteanu, V.M.; Gălățanu, T.; Asztalos, Z.; Gálfi, B.-P. Modern Dimensional Analysis-Based Heat Transfer Analysis: Normalized Heat Transfer Curves. *Mathematics* **2023**, *11*, 741. https://doi.org/10.3390/math11030741

Academic Editor: Lihua Wang

Received: 10 December 2022
Revised: 17 January 2023
Accepted: 28 January 2023
Published: 1 February 2023

1. Introduction

It is well known that the structural elements of civil and industrial buildings must be protected against the unwanted action of fires. Thus, with the occurrence of fires, goods and human beings must be provided with sufficiently large time intervals for evacuation, which directly depends on the fire resistance of the structural elements. This, in turn, is decisively influenced by the way in which they were protected (for example with layers of thermoprotective paints, also called intumescent, etc.), and by the way in which the thermal flow introduced by the fire propagates along the respective structural element.

The previous results of the authors' investigations [1–3], as well as those presented below, facilitate the mastery of this heat flow propagation process along the structural elements.

In a previous paper [3], the authors performed, on an original electric stand [1], a series of experimental investigations of great finesse. The elements subjected to the tests were bars made of steel S275JO, EN 10025:2005, having a full circular section, with a diameter of $d = 0.02$ m and made in different lengths $l = (0.050;\ 0.100;\ 0.150;\ 0.200)$ m.

The bars were electrically heated at one end to achieve nominal temperatures of $t_{O,n} = (100;\ 400)\ ^{\circ}$C. The stand also allowed the positioning of the bars with an angle $\alpha_g = 0^{\circ}$ or 90° from the vertical direction during the experiments.

The bars were equipped with a sufficient number of thermo-couples (FPA15P-type, Ahlborn GmbH, Holzkirchen, Germany), fixed in specially made bores of 0.002 m diameter, which ensured the monitoring of the propagation of the thermal field along them.

In fact, this was the focus of the authors' thorough analysis, i.e., the correlation between $\alpha_n(z)$, m, $\lambda(z)$, as well as its accurate validation. Finally, the authors obtained for each analyzed case one single particular value of "m" along the entire bar.

It should also be emphasized that, based on the curves obtained experimentally under strictly metrological conditions, in [1–3], the magnitudes of the constants $(c_1,\ c_2,\ m)$ could be determined, which are essential elements in the analytical description of the propagation law (1).

Also, the authors proposed an easier, and at the same time, more efficient approach to establishing these constants $(c_1,\ c_2,\ m)$ using the curve-fitting method, where approximation curves of at most order III of the real temperature distribution ensured the same precision as the classical approach based on the laborious (and quite difficult) analysis of the theoretical exponential law. It was also possible to highlight the fact that, with the increase in temperature, this precision of the curve-fitting method increases, even surpassing the classic, exponential one.

Another research direction of the work [3] consisted in the desire of the authors to verify if the hypothesis also remains valid in the case of tubular section bars. In this case, they were made of rectangular tubular bars of steel S355J2, EN 10025:2005. More precisely, they were square pipes, of different lengths, provided with sets of FPA15P-type thermo-couples and subjected to thermal regimes similar to those previously mentioned. According to the authors' knowledge, such investigations, with the aim of verifying the condition of bars having a tubular section, have not been carried out before; at least, we had no knowledge from the specialized literature.

In this way, the authors offered the comparative, effectively measured, thermal distribution laws, with respect to the massive circular (0.016 m in diameter by 0.240 m in length, and 0.020 m in diameter by 0.200 m length), as well as square tubular ($0.040 \times 0.040 \times 0.005$ m by 0.400 m in length) cross-sectional straight bars, having $\alpha_g = 0^\circ$ and $\alpha_g = 90^\circ$, respectively, in angular positioning with respect to the vertical direction, heated at their lower end to nominal temperatures of $t_{O,n} = 100\ ^\circ$C and $t_{O,n} = 400\ ^\circ$C.

These comparative diagrams point out for the engineers involved in fire-protection analysis the importance of the length in the thermal calculi and, based on this, the fire-protecting coating thickness value, too.

The authors proposed a generalized curve, by plotting the relative t_Ψ [%] thermal curve, i.e., monitoring the remaining percentage of the nominal $t_{O,n}$ temperature (considered to represent 100%). These relative t_Ψ [%] thermal curves were plotted for the same initial conditions, and based on the obtained results, several useful conclusions were drawn. One can mention that, based on these relative t_Ψ [%] curves, precisely the same temperature fields were restored in every analyzed case.

The authors also found the very important fact, that in the case of the tubular cross-sectional bars, the $m = const.$ hypothesis for the whole length of the bar is not valid. The hypothesis is valid (can be applied) only for the smallest, constitutive intervals of these tubular bars. In conclusion, the experimentally obtained greater gradients of the thermal distribution law for these tubular cross-sectional bars can be described or drawn up using these "m"-values corresponding to the smallest constitutive intervals.

One other proposed parameter was the so-called compared $\Delta t_\Psi = 100 - t_\Psi$ [%] temperature loss (the percentages of the lost temperatures), which offers a clearer image on the temperature-loss phenomenon.

Based on their graphical images, the increase in the lost Δt_Ψ [%] for the same reference length of ℓ [m] was stated, together with the increase in the bar's total length; this phenomenon was much greater for the horizontally placed bars ($\alpha_g = 90^\circ$), than the vertically positioned one ($\alpha_g = 0^\circ$).

This new parameter assures the most accurate evaluation of the bar's behaviour, having different effective lengths, with respect to the temperature: i.e., its reduction, as well as its propagation along the bars.

Based on the aforementioned strategy, the authors performed thorough analytical calculi of the "m" parameter along these square tubular cross-sectional straight bars for several nominal temperatures: $t_{O,n} = 50;\ 100;\ 200;\ 300;\ 400$; and $500\ ^{\circ}$C.

Using these results, the authors established that an adequate description of the obtained "m"-curves can be obtained by dividing the whole length of the bar into a minimum of three intervals, i.e.: $\ell_{\mathrm{I}} \in [(0 \dots 0.05) \cdot \ell]$; $\ell_{\mathrm{II}} \in [(0.05 \dots 0.10) \cdot \ell]$, and $\ell_{\mathrm{III}} \in [(0.10 \dots 1.00) \cdot \ell]$. These intervals give different gradients and cannot be analyzed together.

The authors, similarly with the t_{Ψ} [%] curve, proposed a new parameter, i.e., *the relative* m_{Ψ} [%] *curve*, which monitors the remaining percentage of the initial value (for $z = 0$) of "m" along the bars' length, considered to represent 100%.

In the same manner, the authors offered a polynomial approach, using a curve-fitting method, both for the global m_{Ψ} [%] curves, as well as for their segmental parts, corresponding to those three separate (detached) intervals.

From this previous contribution [3], as conclusions on m_{Ψ} [%], one can mention the following:

- The greatest gradient for the m_{Ψ} [%] is on the first interval ℓ_{I}, where the obtained gradient is 100 %, that will decrease to 62.3 %; on the second interval ℓ_{II}, there will be a decrease from 62.3 % to 57 %, as well as on the third interval ℓ_{III}, which will decrease from 57 % to 36.8 %;
- Taking into consideration that ℓ_{III} represents, in fact, 90 % of the whole bar length ℓ, the corresponding gradient correlated with its real length is very small;
- For other $t_{O,n}$ nominal temperatures, the mentioned calculi of m_{Ψ} [%] can be performed in a similar manner, which can assure, without difficult analytical calculi, that predictable values for the "m" parameter are obtained;
- In the authors' opinion, these new practical approaches to the temperature distribution law can be applied successfully in the thermal analysis of 2D and 3D structures, in the first stage on reduced scale models, involving the results of the modern dimensional analysis (MDA) (analyzed briefly in the following), as well as in real-scale structures;
- The performed analytical calculi offer a useful tool for fire safety engineers to predict both the heat transfer along the steel structural elements and their load bearing capacity.

The study of structural elements subjected to fire took a new direction with the implementation of dimensional methods in these analyses [4–41].

Starting from the geometric analogy (GA), continuing with the theory of similitude (TS), along with classical dimensional analysis (CDA), the researchers, specialized in problems of preventing the effects of fire, replaced the experimental study carried out directly on the real elements (called prototypes) [39,40,42–65], with that performed on models (usually reduced to scale) [1,2,66–69].

The experimental results obtained on these models could later be transferred to real structural elements based on the relationships provided by the above-mentioned dimensional methods. Thus, the specialists were able to predict the behavior of the prototype based on the measurements made on the model, which obviously represented experiments carried out in much more advantageous conditions in terms of price, cost, working time, specialized personnel, and the equipment involved.

On the advantages and limits of these methods, the authors of this paper made a detailed synthesis of the works [70–74], of which the most significant can be mentioned:

- GA works only with a limited number of laws, based on the identification of points, angles and homologous surfaces of the prototype, in accordance with the related model;
- TS provides an extension of these laws, but can also only be applied to a number of particular cases;
- CDA, although theoretically it would be the ideal method of approach, presents several other shortcomings, such as:

- The deduction of the model law (ML) is based on the processing of a limited number of differential equations related to the phenomenon;
- This processing is unfortunately quite arbitrary, non-unitary, and its efficiency depends to a large extent on the user's experience, usually consisting of grouping some terms of the equations involved, or identifying adimensional groups from the same constitutive equations, in order to obtain dimensionless expressions;
- It requires deep knowledge of higher mathematics, but also of the field of the respective phenomenon;
- Only in particular cases can it provide the complete set of dimensionless variables, based on which the ML is later defined;
- The method, not being unitary in approach, is not easily applicable to ordinary researchers, remaining accessible only to a narrow segment of established specialists.

As is well known, both TS and CDA operate with a set of dimensionless variables π_j, $j = 1, 2, \ldots, n$, from which the ML will ultimately result.

Also, the number of dimensionless expressions, which can thus be obtained from a limited number of differential equations related to the phenomenon, will also be limited. This is why CDA cannot provide, except in very particular cases, the full set of the ML through these dimensionless variables.

In order to eliminate these shortcomings, as well as to make dimensional analysis an accessible and effective method for ordinary researchers, Th. Szirtes developed a new approach, which gave rise to the so-called modern dimensional analysis (MDA) [75,76].

Among the indisputable advantages of MDA, the following can be highlighted:

- The method is unitary, simple and accessible to any researcher;
- It does not require thorough knowledge in the field, but only that all the parameters are taken into account, which can in a certain way have an influence on the respective phenomenon;
- The parameters, which have no influence on the phenomenon, are automatically removed from the protocol;
- The complete set of dimensionless variables is always provided, and consequently also the complete ML;
- The developed method is very flexible, allowing, based on the ML deduced for the general case, customizations to be made in order to simplify and optimize the model, as well as the related experiments;
- MDA allows choosing at will the set of variables that define the protocol of experiments on the model, but also the model itself.

MDA was also successfully applied by the authors of this paper, among others, in the analysis of the stressed-strained states of the reticular structures in constructions [77], but also in the detailed study of the thermal field propagation phenomenon [70–73,78], for those tracking the simulated effect of fires on original stands designed and made by them [2,47,72,78,79].

One might ask, why did the authors use the MDA in these investigations?

The reason was that only the further application of such research to firm and reliable laws such as those provided by MDA can ensure a firm correlation between the behavior of a prototype and its associated model.

Thus, if much simpler, safe and repeatable investigations are desired to be carried out on the associated model and to form a solid basis in predicting the behavior of the prototype, then this safe method, i.e., MDA, must be involved.

Consequently, the authors, in their previous works [70,72,78,79], proposed and performed the validation of the model law deduced not only for the case of the solid circular section bar, but also for the one with tubular-rectangular section, with the implicit and obvious particular case of the tubular-square section.

Based on the ML deduced for the rectangular-tubular section, the authors performed a thorough validation study regarding the thermal regimes of a prototype, which was the column segment of a real pillar in an industrial hall, using models reduced to scales of 1:2; 1:4 and 1:10.

In the following, the major aspects of these experimental investigations, which were the basis for establishing the thermal propagation curves along the tested structural elements, are briefly presented.

As will be seen below, the analysis of these thermal curves through a new lens allowed a much more efficient approach, which is in fact the main purpose of this work.

2. Materials and Methods

In order to carry out these theoretical-experimental investigations, for the first time the authors designed an original electrical stand [2,71,72,79]. This stand, with a high-performance electronic control, ensures precise monitoring and control of the heating of structural elements, made either on a natural scale or on a reduced scale.

The ML, deduced for the case of structural elements with tubular-rectangular sections [73], was validated based on a significant number of experimental measurements, both on the analyzed prototype and on the associated models, made at 1:2, 1:4, and 1:10 scales [2,71,72,80].

According to the works [2,71,72,78], the scheme of these structural elements, as well as the location of the temperature sensors, which were PT100-420 thermoresistors with 150 mm long terminals, having a working temperature between −70 and +500 °C, are shown in Figures 1–3, and Table 1. The thermoresistors were fixed to the structural elements with the help of M3 screws in precisely positioned threaded holes.

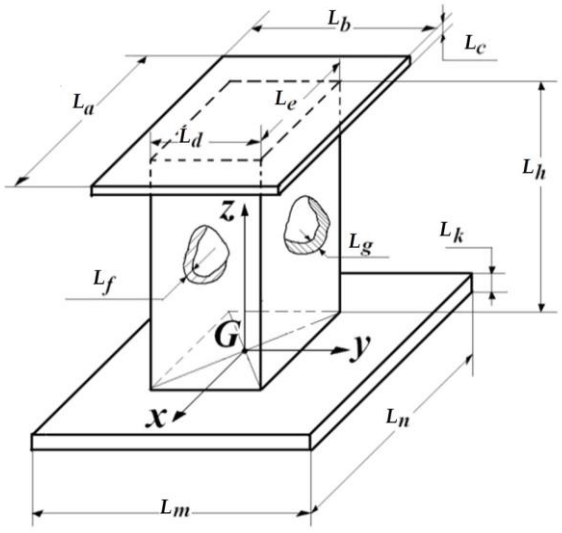

Figure 1. Dimensions of the column segment [2,71,72,78].

The geometric similarity is respected in all of them, accepting the same scales of all dimensions of 1:1, 1:2, and 1:4.

The upper closing plate, with the dimensions $(L_a \times L_b)$, substitutes the rest of the column, and the lower one, with the dimensions $(L_m \times L_n)$, assures a perfect and unitary placement of all the elements tested on the test stand.

Table 1. Principal dimensions of the column segment presented in Figure 1 [2,71,72,78].

	Prototype, at Scale 1:1	Model I, at Scale 1:2	Model II, at Scale 1:4
	Dimensions, in m		
L_a	0.370	0.185	0.0925
L_b	0.370	0.185	0.0925
L_c	0.006	0.003	0.0015
L_d	0.350	0.175	0.0875
L_e	0.350	0.175	0.0875
L_f	0.016	0.008	0.004
L_g	0.016	0.008	0.004
L_h	0.400	0.200	0.100
L_k	0.010	0.005	0.0025
L_m	0.450	0.450	0.450
L_n	0.450	0.450	0.450

The structural element (1) from Figure 2, is placed by translation on the upper area of the truncated pyramid-shaped dome (2); this dome rests on the rigid frame (3) and on the supporting legs (4).

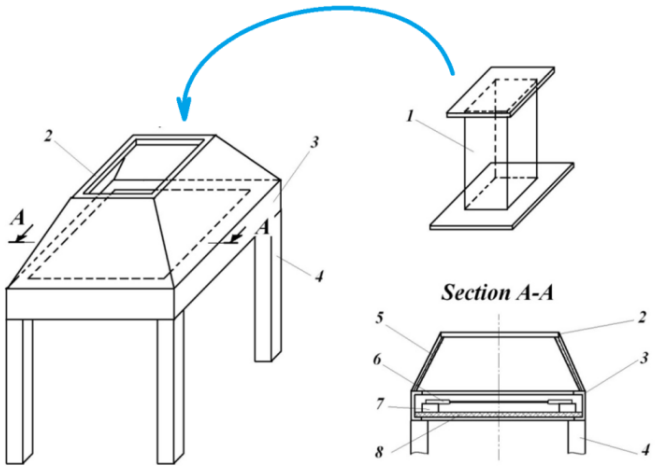

Figure 2. The assembled stand [2,71,72,78].

During experimental investigations, the free surface of the laying board with dimensions $(L_m \times L_n)$, shown in Figure 1, is covered with a thermal insulation blanket. As an illustration of the degree of thermal insulation, it can be mentioned that at the nominal heating temperature of $t_{o,nom} = 600\ ^{\circ}\mathrm{C}$ for the tested structural elements, around the support frame (3) and the truncated pyramid (2), the temperature did not exceed $(45 \ldots 50)\ ^{\circ}\mathrm{C}$. In section A–A the heating elements (6) are shown, consisting of twelve silite rods, each four connected in series for the three phases of the industrial power supply at 380 V. These silite rods, placed on chamotte bricks (7), rest on a thermal insulation layer (8) of ceramic fiber 0.0254 m thick. A similar insulation (5), provided for the lateral sidewalls of the truncated pyramid (2), assures an efficient thermal insulation of the test bench (see Table 2).

Table 2. Principal coordinates of the temperature measuring points [2,71,72,78].

Prototype, at Scale 1:1	Model I, at Scale 1:2	Model II, at Scale 1:4	Model III, at Scale 1:10
Coordinates *z*(*j*) in m			
0.020	0.020	0.020	0.015
0.110	0.060	0.055	0.030
0.200	0.105	0.090	0.045
0.290	0.150		0.060
0.380	0.190		0.100
			0.200
			0.400
			0.460
			0.495

A thermo-couple was always placed at the coordinate level $z(0)$, which also ensured the implicit control of the nominal temperature $t_{O,nom}\ [^{\circ}\mathrm{C}]$.

The important fact should be mentioned that, at the time of carrying out the tests on the first three elements, i.e., on the prototype and the models made at the scales of 1:2 and 1:4, the results of the theoretical-experimental investigations carried out on the first tubular structural elements, synthesized, were not yet known in our previous article [3].

As mentioned in Section 1, these investigations, reproduced in the work [3], demonstrated the fact that, in the case of tubular sections, the hypothesis $m = const.$ is valid only on constitutive areas of the length of the bar, which is why the respective bar must be divided into at least three subintervals, for which, subsequently, this assumption will be respected individually.

The tests on the last model reduced to the scale of 1:10 were carried out after the completion of the theoretical-experimental investigations presented in the authors' previous work [3], which is why it was already possible here to take into account this important conclusion regarding the validity of the hypothesis $m = const.$ on subintervals.

Figure 3 shows the mounting on the aforementioned testing bench of the thin tubular-rectangular tested specimen (frame column), manufactured at 1:10 scale [71,72,78,79].

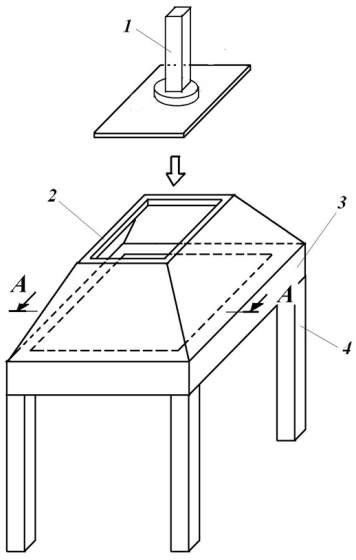

Figure 3. Heating stand, together with the tested 1:10 scale pillar model.

The dimensions of this reduced scale model are $0.030 \times 0.030 \times 0.0015$ m, and its height is 0.5 m. This model presents on its lower end a steel cylindrical part with diameter $d = 0.105$ m and height $h = 0.015$ m, by means of an intermediate $0.080 \times 0.080 \times 0.003$ m steel plate (Figure 4).

The significant thermal inertia of this cylindrical part assures the corresponding heat transfer from the testing bench to the reduced-scale tubular model.

A 0.025 m thick heat-insulation open cylinder, with 0.45 m diameter and 0.65 m height, disposed around the tested element, eliminates the undesirable influence of an accidental current of air from the lab. The radius of this heat-insulation cylinder is comparable, at the reduced scale of 1:10, with the half-distance between the columns.

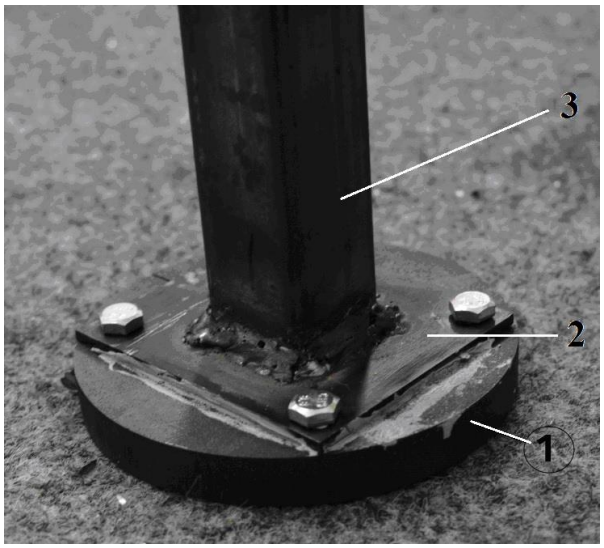

Figure 4. The lower end of the thin-walled tested element (column): 1—cylinder; 2—intermediate plate; 3—tested element (column).

The thermal protection of the elements subjected to the tests was carried out with the help of solvent-based intumescent paint (Interchar 404, from International Marine and Protective Coatings), applied with a thickness of 1.2 mm.

The thermal regimes imposed on the first three elements, i.e., of the prototype and the models reduced to the 1:2 and 1:4 scale, were at the nominal temperatures $t_{0,nom} = (100,\ 200,\ 300,\ 400,\ 450,\ 500)\ ^{\circ}\mathrm{C}$, and the nominal temperatures for the element made at the 1:10 scale, were $t_{0,nom} = (100,\ 200,\ 300,\ 400,\ 450,\ 500,\ 600)\ ^{\circ}\mathrm{C}$.

The protocol of these heatings, i.e., their evolution over time, for both thermally unprotected and thermally protected elements, according to the paper [71], is shown in Figures 5–12. Here, for the thermoresistors located at different heights, their indications were specified, i.e., the temperatures stabilized at their level, corresponding to the imposed nominal temperatures $t_{0,nom}\ [^{\circ}\mathrm{C}]$.

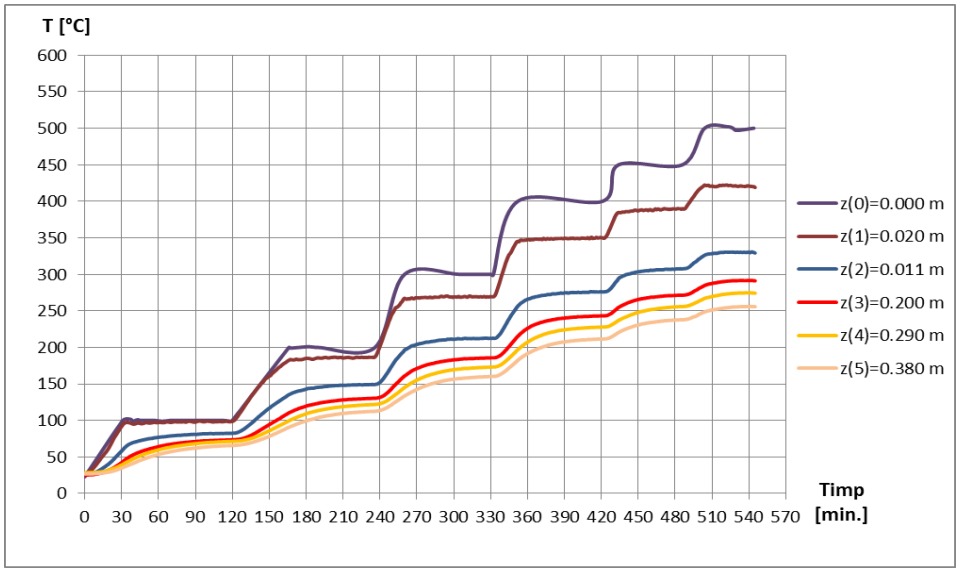

Figure 5. Time evolution of the temperature in the unpainted prototype.

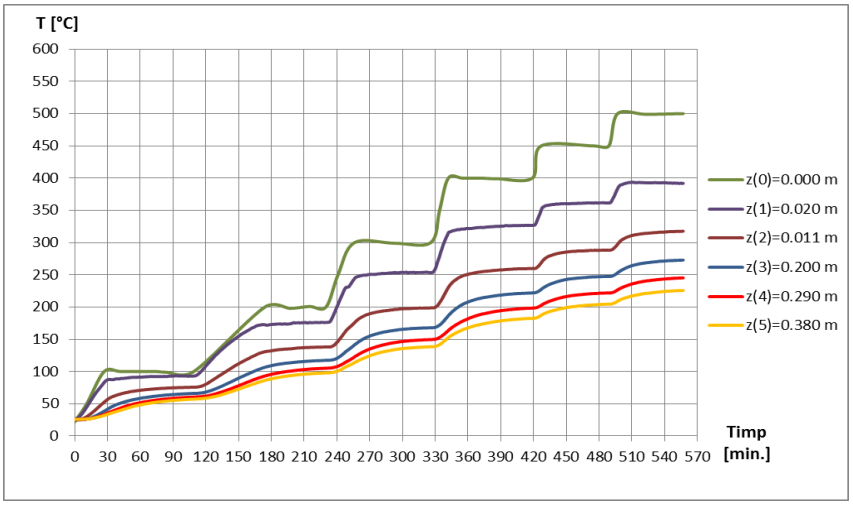

Figure 6. Time evolution of the temperature in the painted prototype.

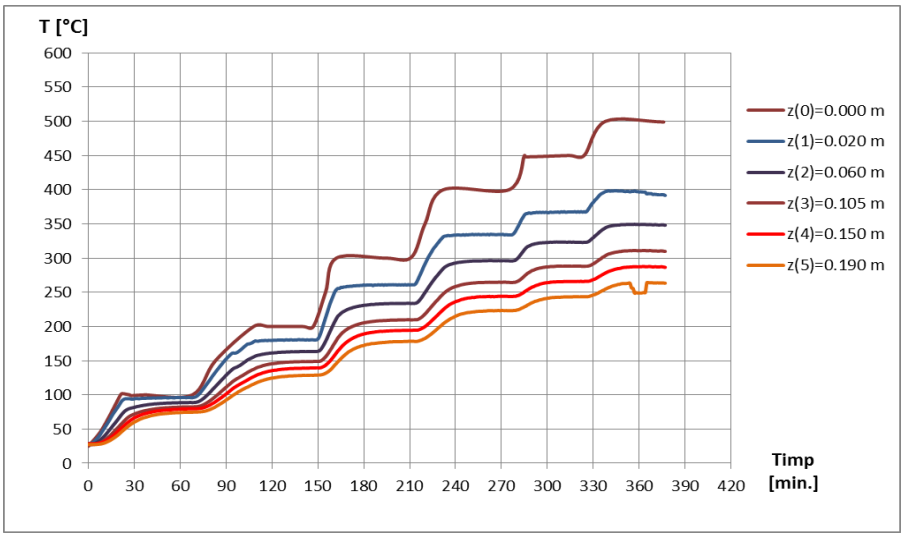

Figure 7. Time evolution of the temperature of the unpainted 1:2 scale model.

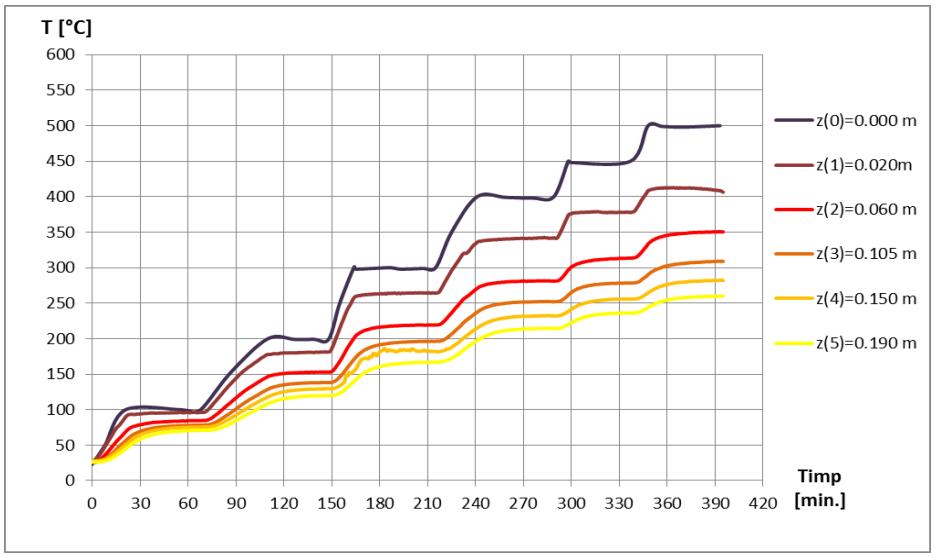

Figure 8. Time evolution of the temperature of the painted 1:2 scale model.

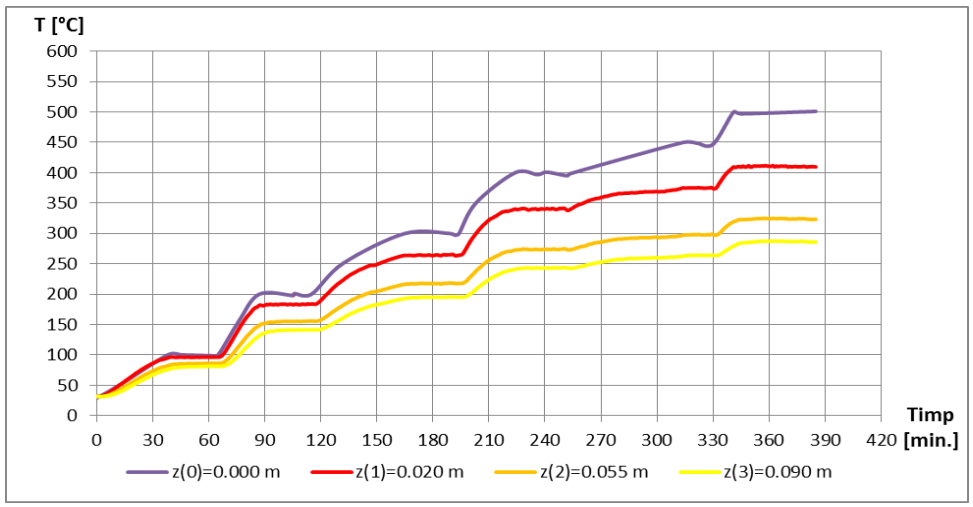

Figure 9. Time evolution of the temperature of the unpainted 1:4 scale model.

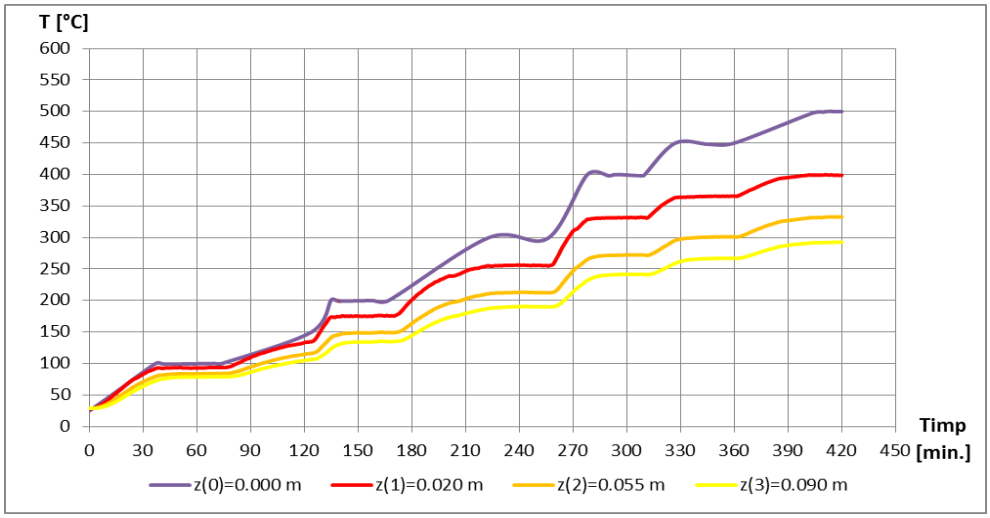

Figure 10. Time evolution of the temperature of the painted 1:4 scale model.

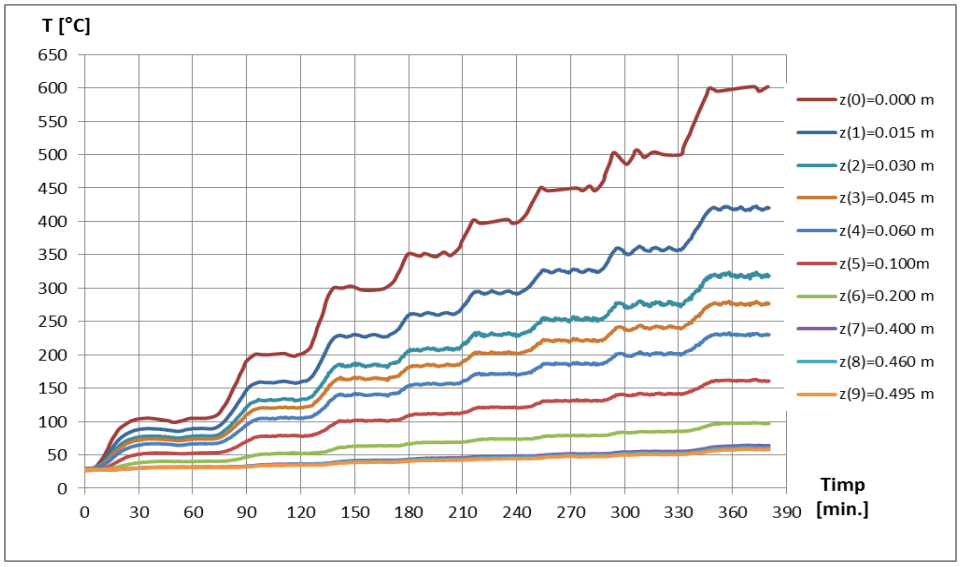

Figure 11. Time evolution of the temperature of the unpainted 1:10 scale model.

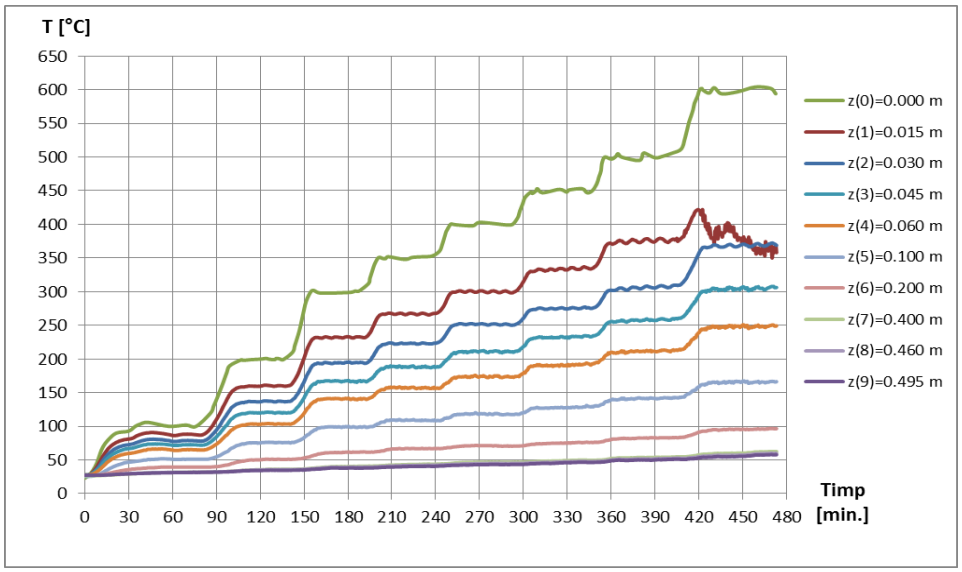

Figure 12. Time evolution of the temperature of the painted 1:10 scale model.

It can be seen that, at the end of each heating step, there is a temperature stabilization level; the monitoring of the temperatures along the elements subjected to the tests was carried out only after the completion of the respective stabilization cycle.

3. Results

In Figures 13–18, the results of monitoring the thermal field with the help of thermoresistors mounted on these structural elements are provided (see [71]).

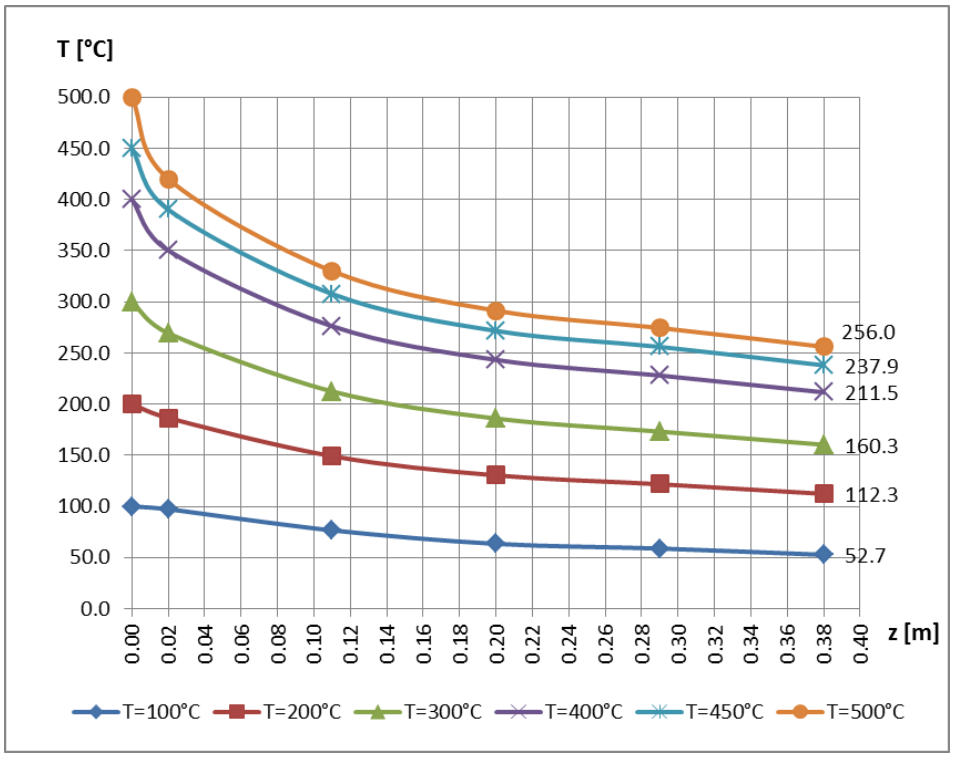

Figure 13. Temperature variation along the unpainted prototype.

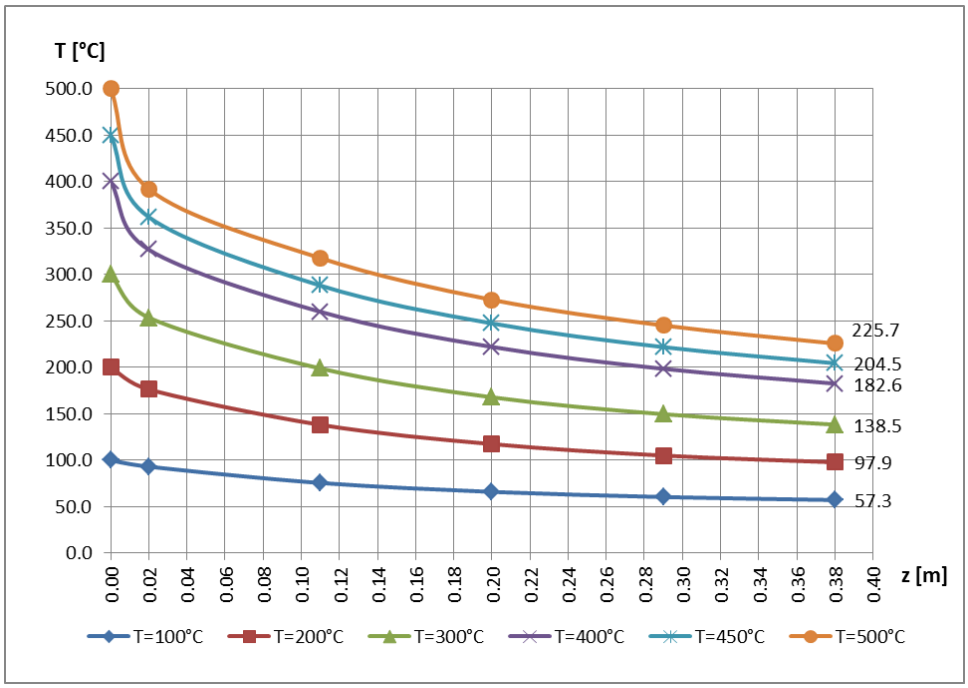

Figure 14. Temperature variation along the painted prototype.

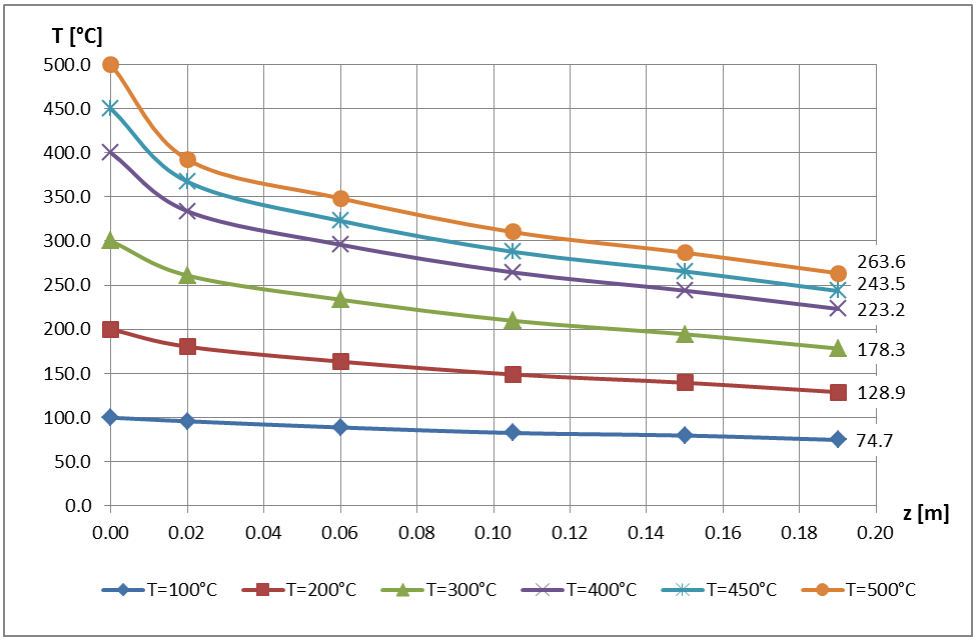

Figure 15. Temperature variation along the unpainted 1:2 scale model.

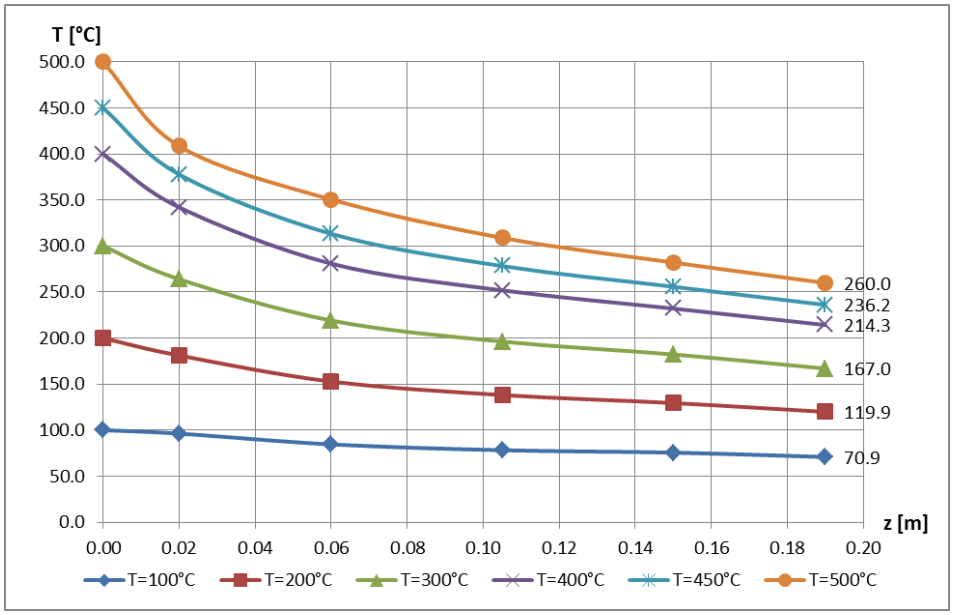

Figure 16. Temperature variation along the painted 1:2 scale model.

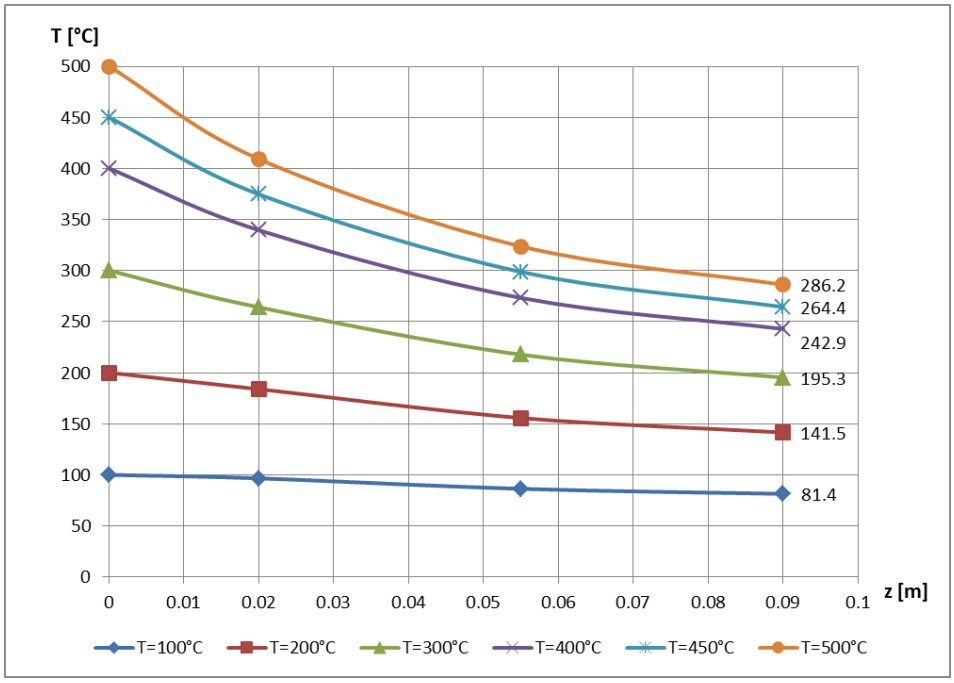

Figure 17. Temperature variation along the unpainted 1:4 scale model.

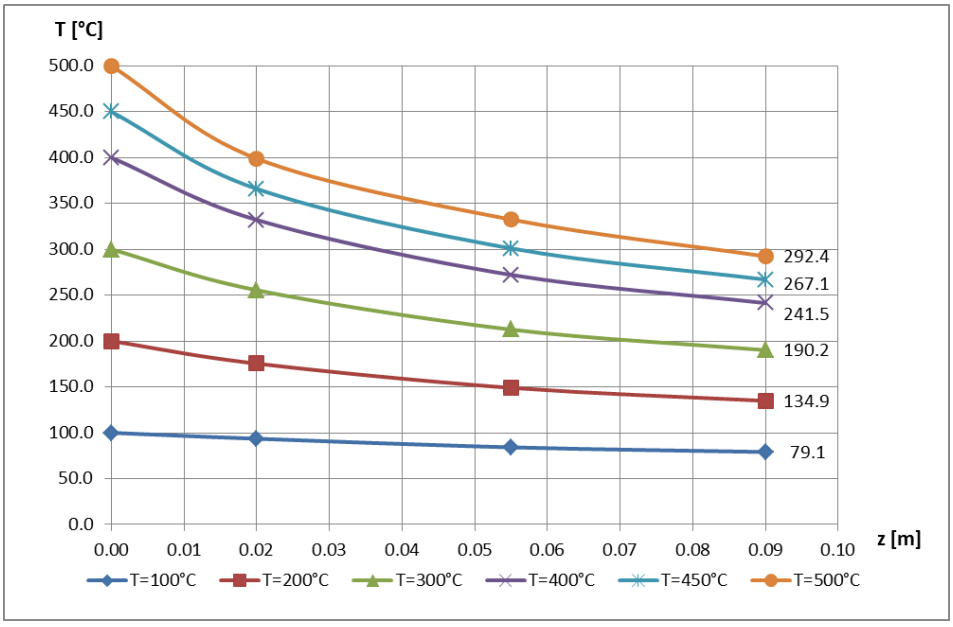

Figure 18. Temperature variation along the painted 1:4 scale model.

In Figures 19 and 20 it can be seen that the thermoresistor, located at a distance of $z = 0.015$ m, presented a deficiency in operation, which is why its last recording could not be taken into consideration during the subsequent processing of the data.

It should also be mentioned that the last structural element, made at a scale of 1:10, actually represented the model attached to the entire pillar.

Starting from this fact, and taking into account the results obtained and presented in the work [2], we proceeded to divide the curves related to this model reduced to a scale of 1:10 into three intervals, according to those in Section 1, i.e., $\ell_{\mathrm{I}} \in [(0 \ldots 0.05) \cdot \ell] = [0 \ldots 0.03]$ m; $\ell_{\mathrm{II}} \in [(0.05 \ldots 0.10) \cdot \ell] = [0.03 \ldots 0.06]$ m, and $\ell_{\mathrm{III}} \in [(0.10 \ldots 1.00) \cdot \ell] = [0.06 \ldots 0.50]$ m.

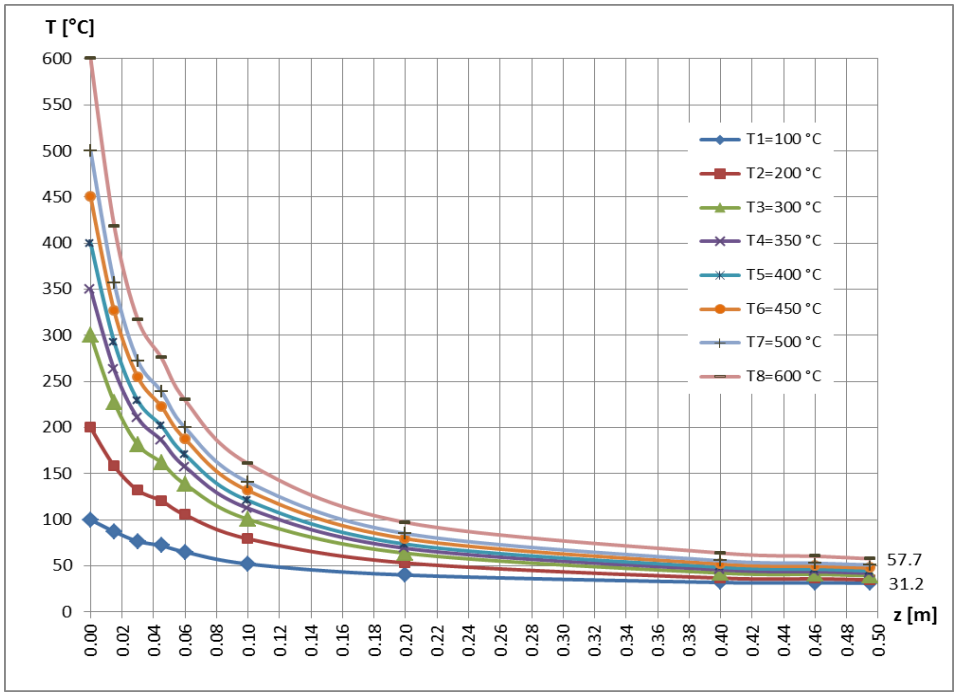

Figure 19. Temperature variation along the unpainted pole, made at 1:10 scale.

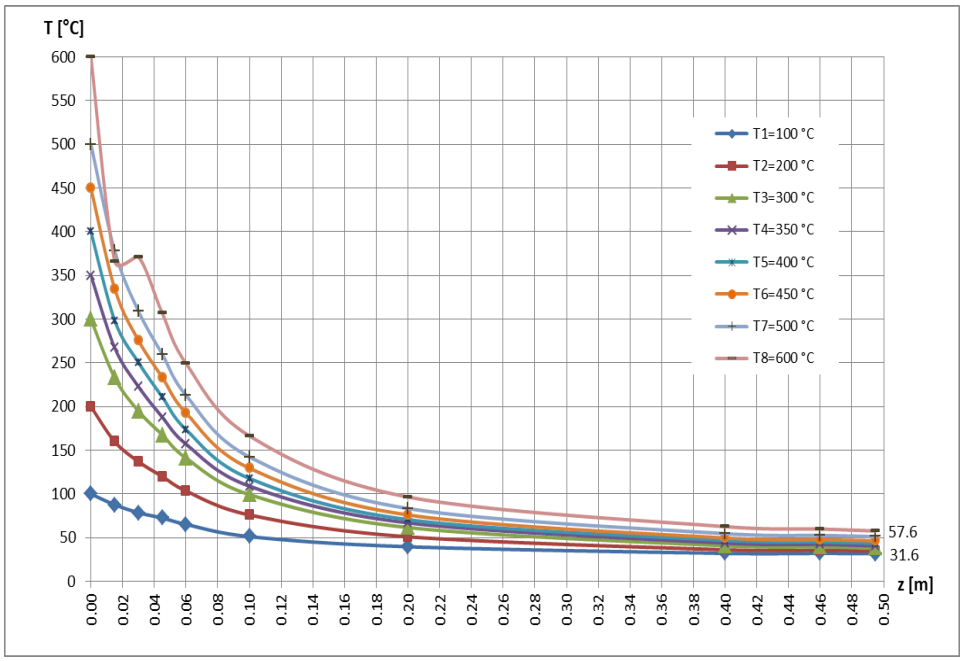

Figure 20. Temperature variation along the painted pole, made at 1:10 scale.

Later, based on this subdivision, the respective curves obtained through experimental measurements could be approximated each time with minimum degree polynomial functions; these results are analyzed in Section 4.

Figure 21a–c show these new intervals related to the curves in Figure 19, and in Figure 22a–c, those corresponding to the curves in Figure 20.

At first glance, the curves in Figures 21c and 22c would show strong gradients of temperature variation, but if one carefully follows the z(m) scale, one notices that, in fact, these lengths are much larger than at the first two sets of diagrams (Figures 21a,b and 22a,b); consequently, these last intervals actually show very smooth changes in temperatures on

the portion The faulty behavior of the above-mentioned thermoresistor can also be seen on Figure 22a; here, in fact, the processing of the initial curve from Figure 20 was carried out.

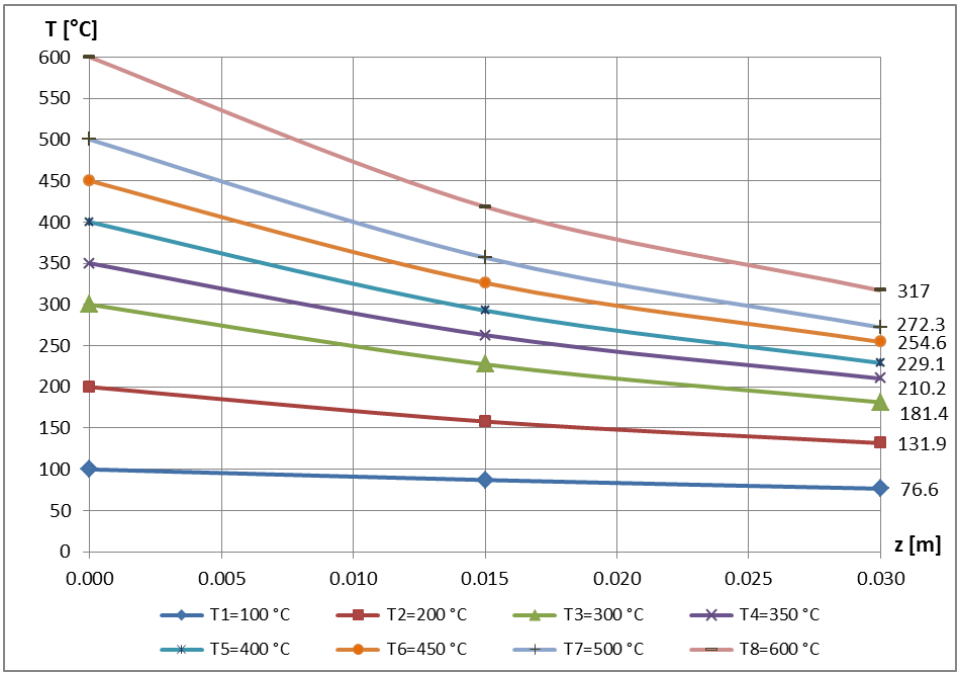

(**a**)

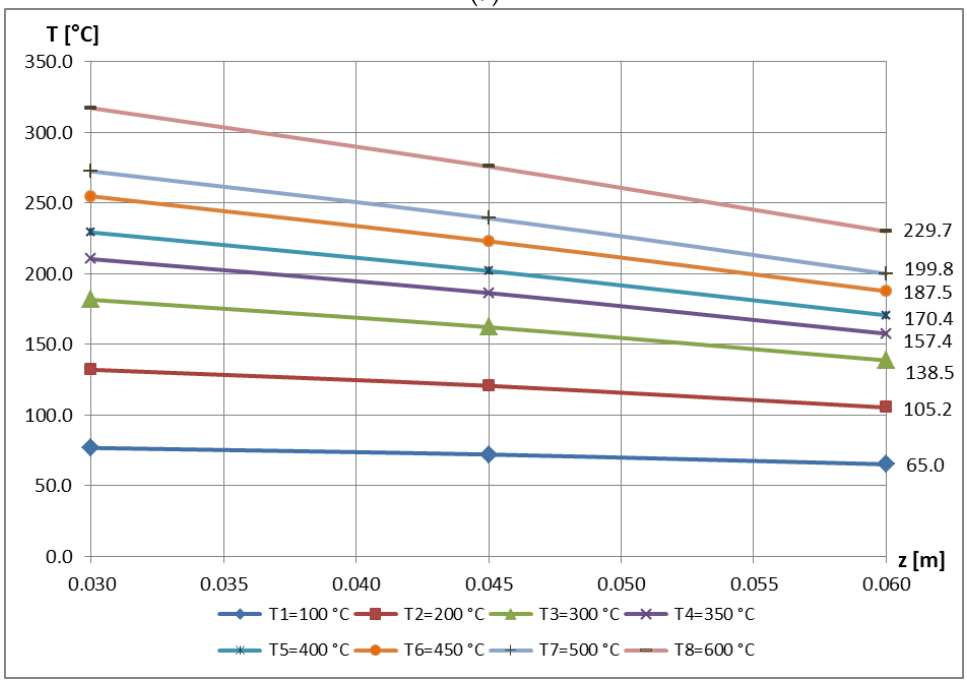

(**b**)

Figure 21. *Cont.*

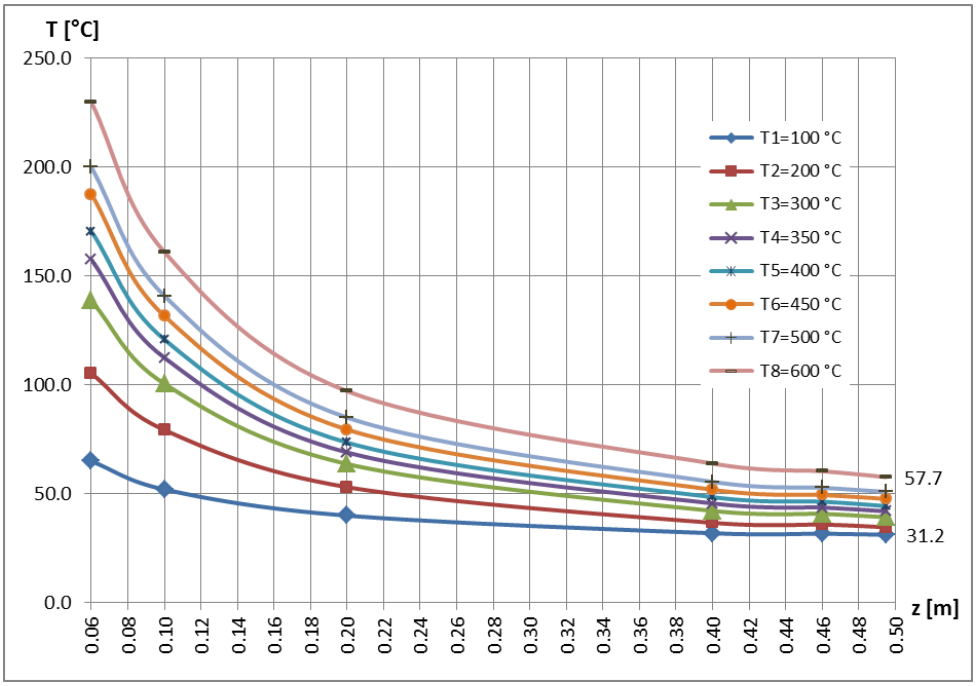

(**c**)

Figure 21. Variation of temperature along the intervals of the unpainted base, made at a scale of 1:10, according to Figure 19: (**a**) ℓ_{I}; (**b**) ℓ_{II}; (**c**) ℓ_{III} [71].

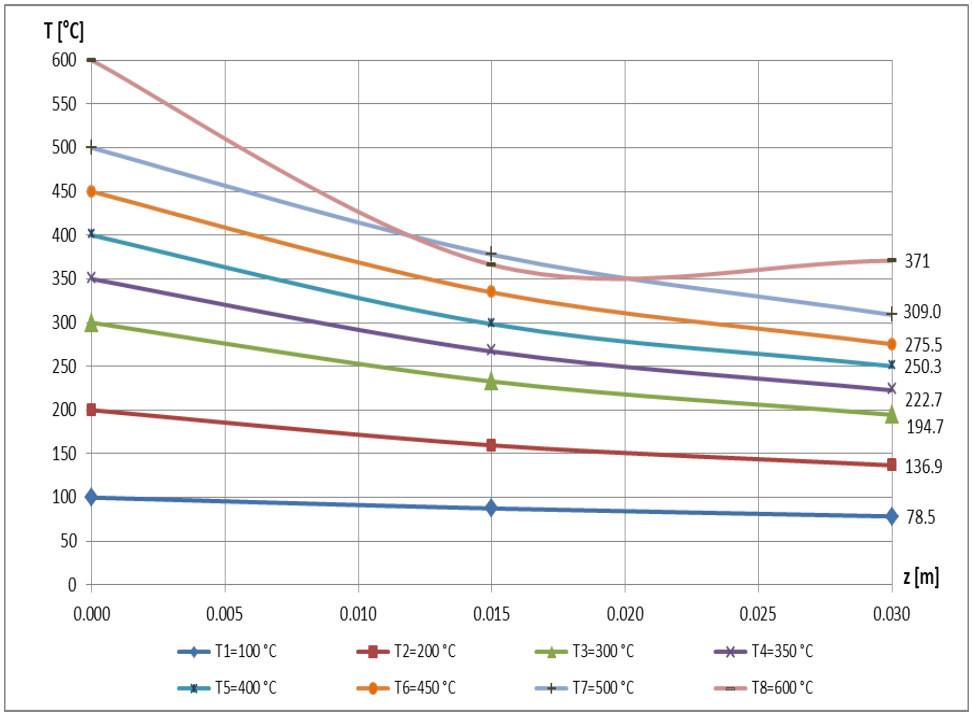

(**a**)

Figure 22. *Cont.*

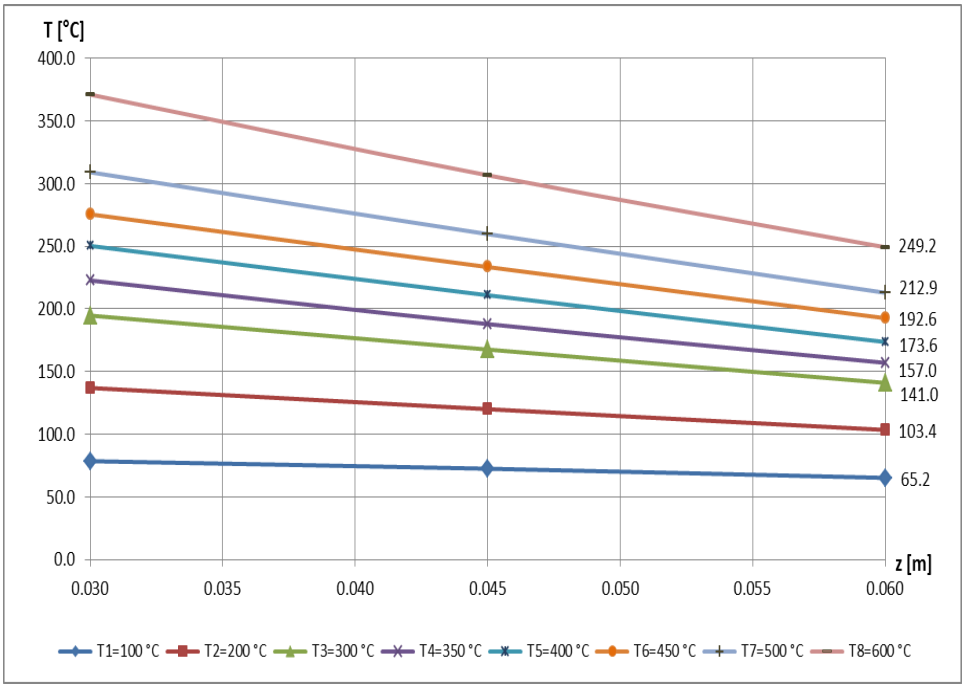

(**b**)

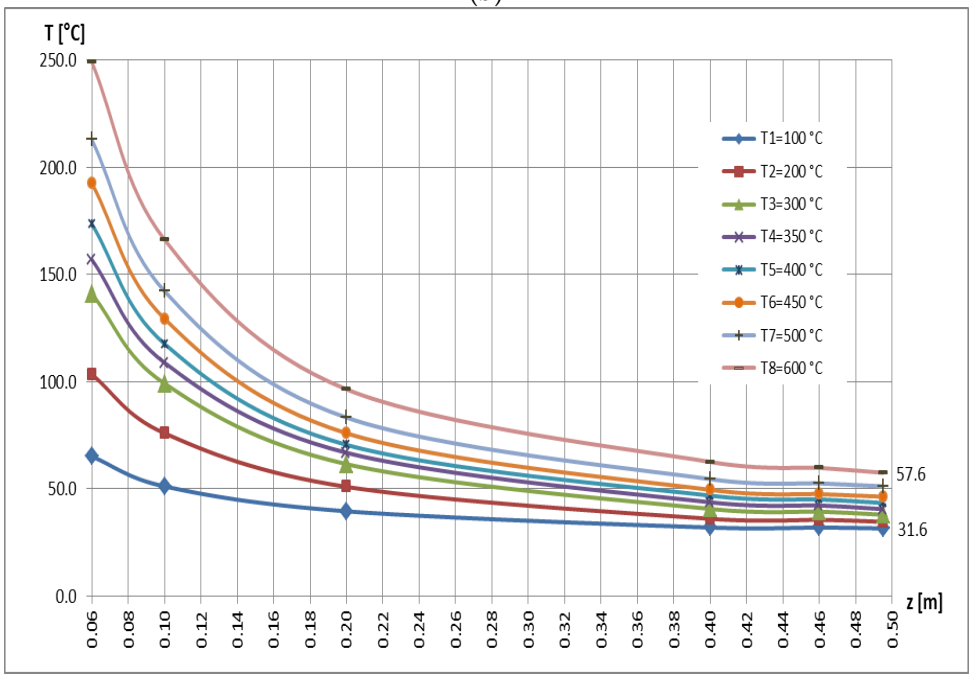

(**c**)

Figure 22. Variation of temperature along the intervals of the painted pillar, made on a scale of 1:10, according to Figure 20: (**a**) ℓ_{I}; (**b**) ℓ_{II}; (**c**) ℓ_{III} [71].

4. Discussion

In the previous paper [3], the classical, exponential, and the polynomial approach to temperature variation curves, curves obtained based on rigorous measurements, was presented.

New parameters were proposed, namely: the relative thermal curve t_{ψ} [%] as well as the compared temperature loss $\Delta t_{\psi} = 100 - t_{\psi}$ [%] (the percentages of the lost temperatures). Also, also in the work [2] a more effective methodology for establishing the "m"

parameter was proposed, but also the proposal of a new parameter, i.e., the relative curve m_{ψ} [%].

These results, as mentioned before, also facilitate the calculation of the heat transfer coefficient α_n, which, as is well known, is a major objective of these analyses.

The authors performed high-accuracy metrological measurements of the involved heat/temperature sensors' accuracy, namely, of the PT 100-type thermoresistors. In Figure 23 the original testing device of these thermoresistors' accuracy is shown. From the literature, it is a well-known fact that the thermo-couples have, in practice, high-accuracy sensors, up to class 0.1. Because the involved PT 100 thermoresistors present a lower accuracy, the authors first performed a comparative analysis of them with such a calibrated thermo-couple.

A steel disc, with a 105 mm diameter and a height of 15 mm, manufactured from the same quality steel as the associated elements in the described experiments from the present contribution, was designed with a central hole with a 2 mm diameter (destined for the thermo-couple fixing) and with three other *M3* screws disposed symmetrically for the PT 100 thermoresistors. By applying the same thermo-charging (heating them up to the same temperatures as the involved sensors in the described experiments), their own calibration curves were drawn up with respect to the thermo-couple's indication, as well as a probable (global) calibration curve, i.e., with their mean values. Consequently, by this preliminary calibration, the thermal deviation of the involved PTs was stated with respect to the real indicated values (by means of a high-accuracy thermo-couple). All collected data during the experiments mentioned in the paper were corrected, taking into consideration the obtained thermal deviation.

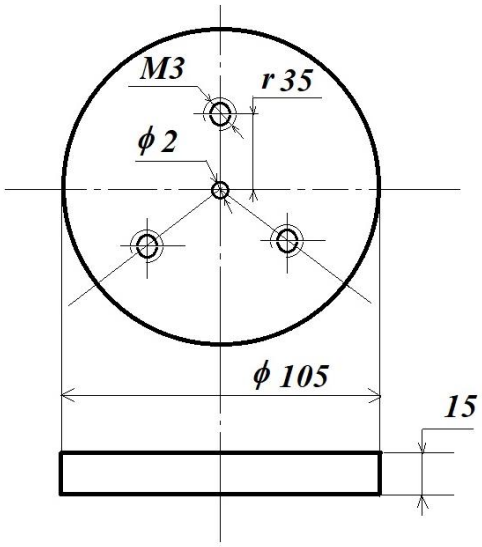

Figure 23. The testing device of the comparative accuracies (dimensions are in mm).

One other supplementary approach to the measurements' uncertainty consisted in performing a metrological evaluation for each channel of the involved data acquisition chain, starting from the thermoresistor, a LABJACK 9 acquisition device, up to the laptop.

In this way, different high-accuracy (class 0.1) electrical resistors substituted each PT in order to obtain for the whole thermal interval (up to 600 °C) the corresponding electrical signals for all involved channels. Based on these indications a second re-calibration of the collected electrical signals from each PT became possible.

One can conclude that this re-calibration was performed the first time by the above-mentioned comparative measurements of the calibrated thermo-couple vs. three PT 100 thermoresistors, and afterwards, based on these electrical resistors' indications.

In the authors' opinion, the obtained data can be considered acceptable from the point of view of metrological accuracy, as well as uncertainty.

To obtain a more comprehensive (more general) approach, the authors propose introducing a percentage length L_ψ [%] instead of the effective length $z(\mathrm{m})$; this new length considers the value of 100% of the size of the quota $z_{\max}$. With the help of this new parameter, Figure 24 shows the curves related to the nominal temperature $t_{0,nom} = 400\ ^\circ\mathrm{C}$ for the first three unpainted structural elements (not thermally protected), i.e., the prototype, and the models reduced to the scales of 1:2 and 1:4; these curves are extracted from Figure 13, Figure 15, Figure 17 respectively, and analyzed with the percentage length L_ψ [%].

Similarly, in Figure 25 the related curves of the same structural elements are shown, but thermally protected, i.e., painted; these resulted by extracting data from from Figure 14, Figure 16, Figure 18 respectively, and analyzed with the help of L_ψ [%].

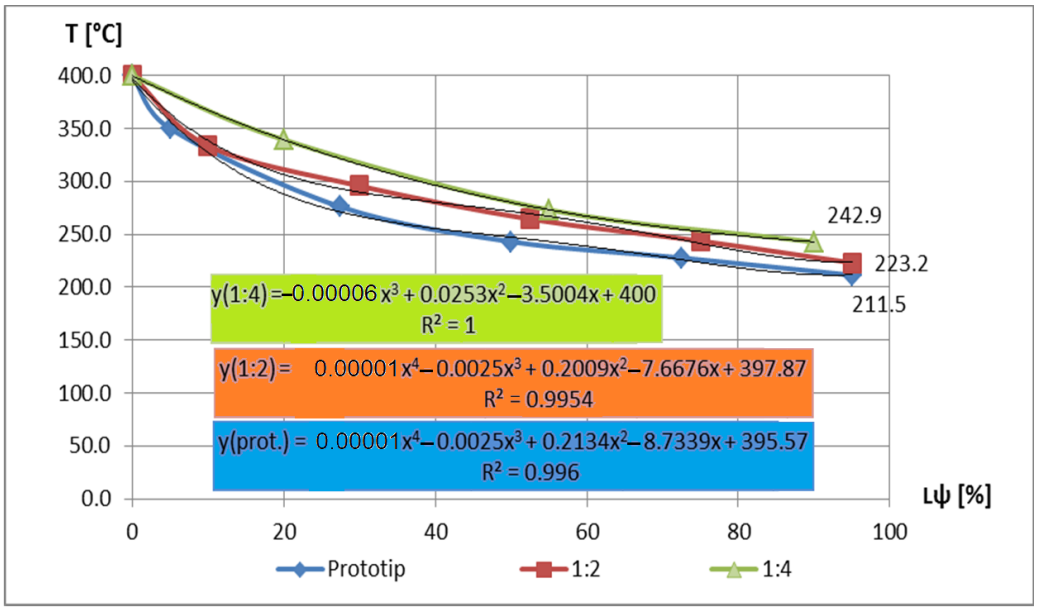

Figure 24. The three segments of unpainted columns, at 400 °C [71].

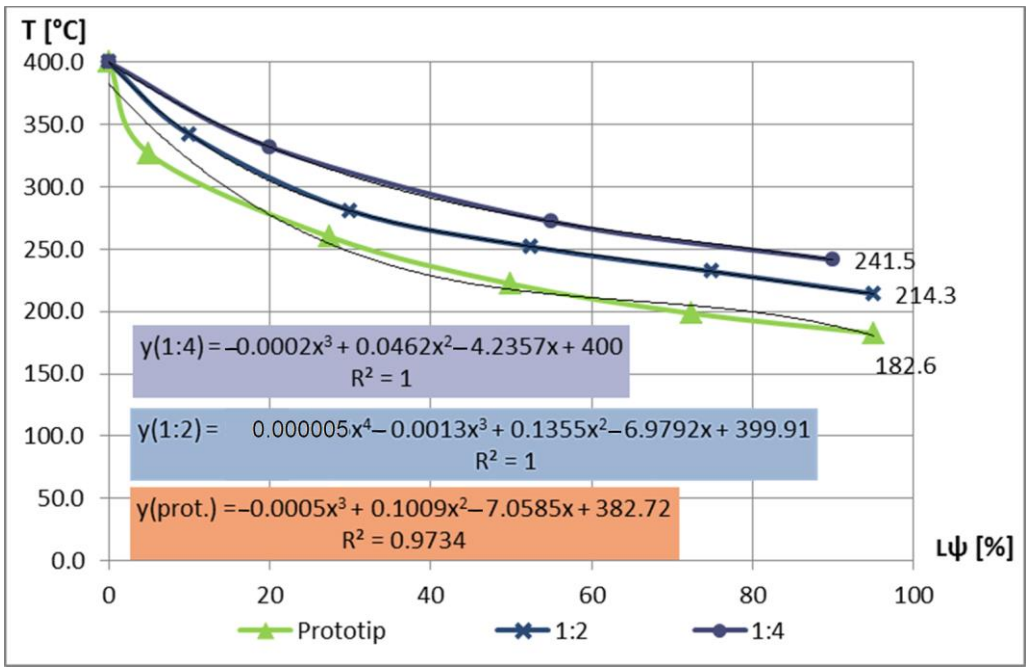

Figure 25. The three segments of painted columns, at 400 °C [71].

One can notice a very similar allure of the curves rendered within the same figure, although their sizes and volumes were very different. In the same figures, the approximation polynomial curves are also mentioned, of the order IV at most, but with a very good correlation factor R^2.

A similar approach in the case of the pillar reduced to a scale of 1:10 led to obtaining the curves in Figure 26, according to Figure 19, and its more precise analysis of the subintervals, corresponding to the nominal temperatures of $t_{0,nom} = 400$ °C and $t_{0,nom} = 500$ °C, shown in Figures 27–29. It can be noted that the change in the degree of the approximation polynomial functions with the analyzed subinterval depends on the gradient of the initial temperature curves.

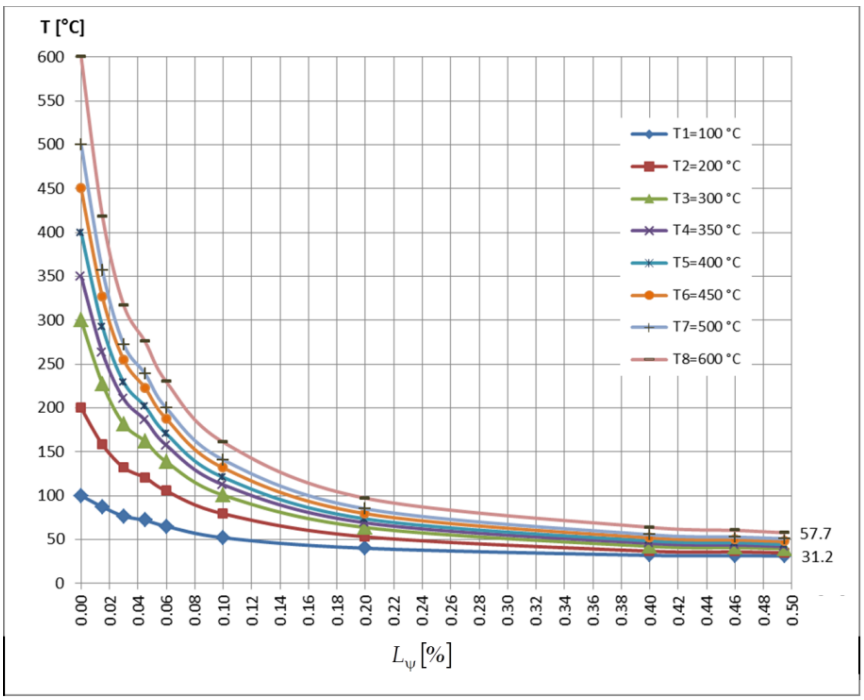

Figure 26. Temperature variation along the unpainted pole, made at 1:10 scale.

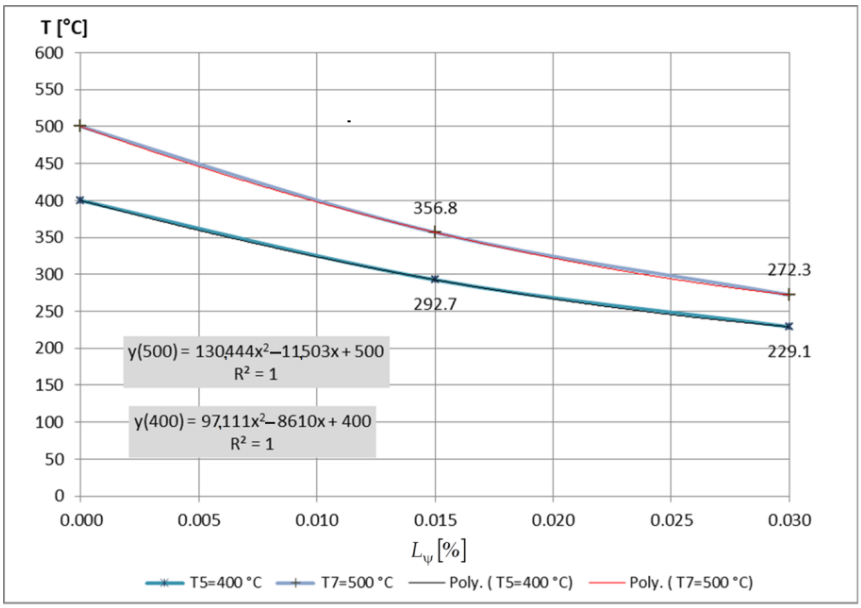

Figure 27. Variation of temperatures along the painted pole, made at 1:10 scale; the first interval in Figure 26.

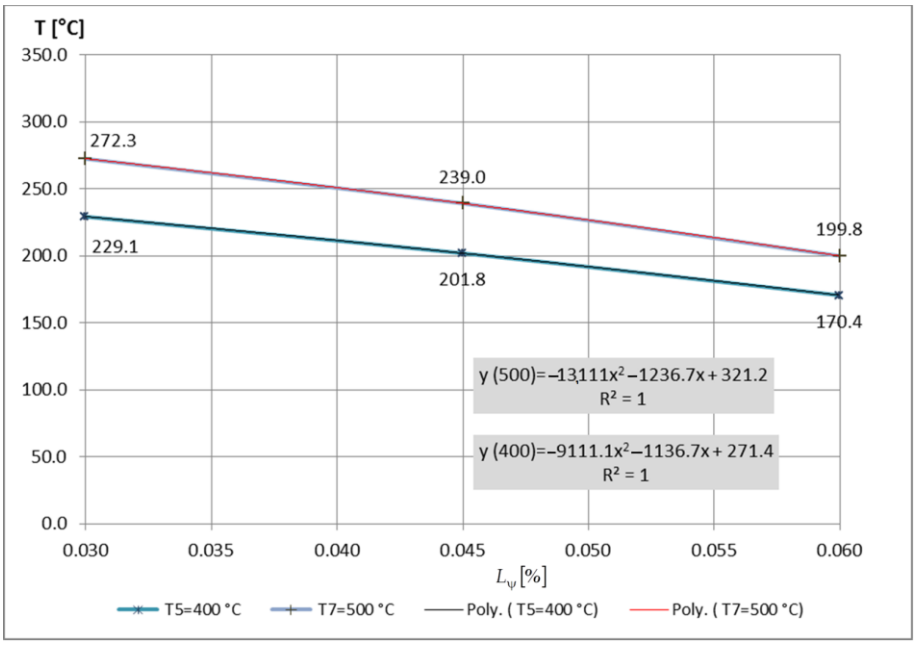

Figure 28. Variation of temperatures along the unpainted pole, made at 1:10 scale; the second interval in Figure 26.

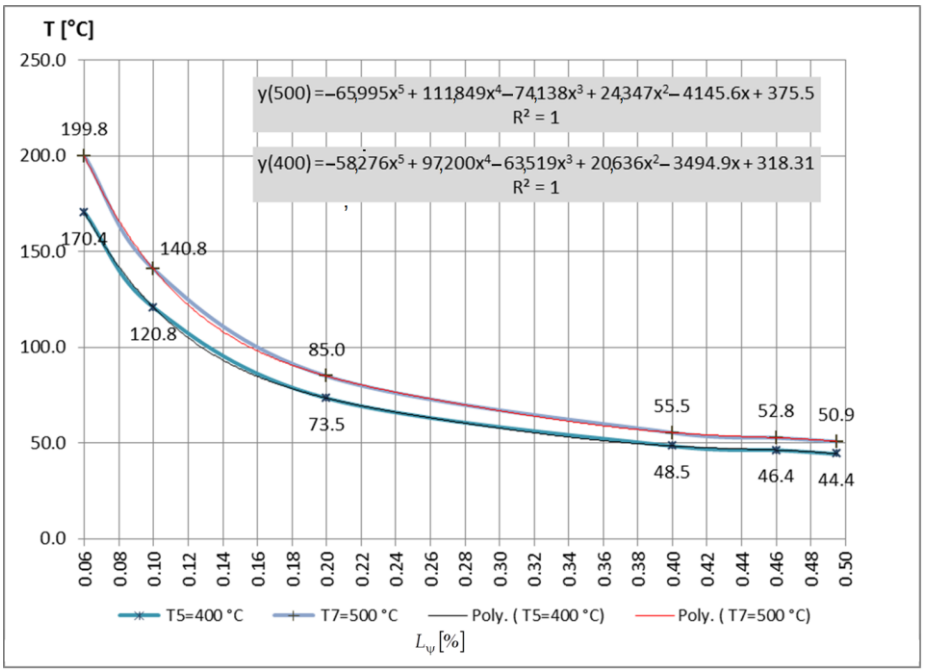

Figure 29. Variation of temperatures along the painted pole, made at 1:10 scale; the third interval in Figure 27.

If on the first subinterval, related to ℓ_I, the gradient is too strong, then one can use an additional division of it into two other units in order not to excessively increase the degree of the approximation polynomial, but also to keep a better correlation factor as R^2.

A similar analysis for the painted 1:10 scale pillar is shown in Figure 30, according to Figure 20, and its more precise analysis of the subintervals, corresponding to the same nominal temperatures of $t_{0,nom} = 400\ ^\circ$C and $t_{0,nom} = 500\ ^\circ$C, is shown in Figures 31–33.

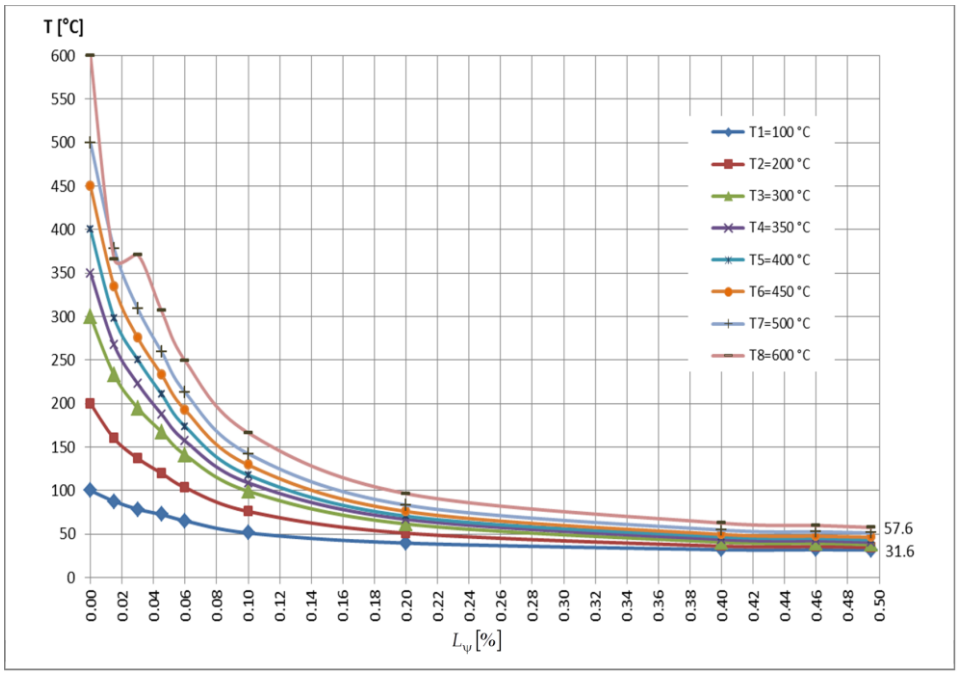

Figure 30. Temperature variation along the painted pillar, made at 1:10 scale.

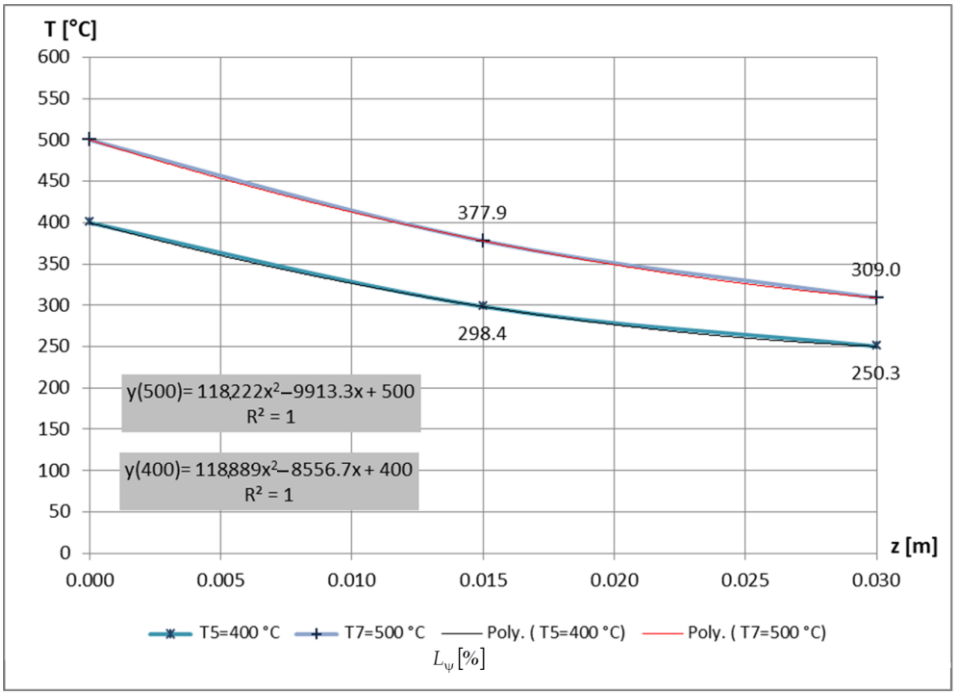

Figure 31. Temperature variation along the painted pole, made at 1:10 scale, for the first interval in Figure 30.

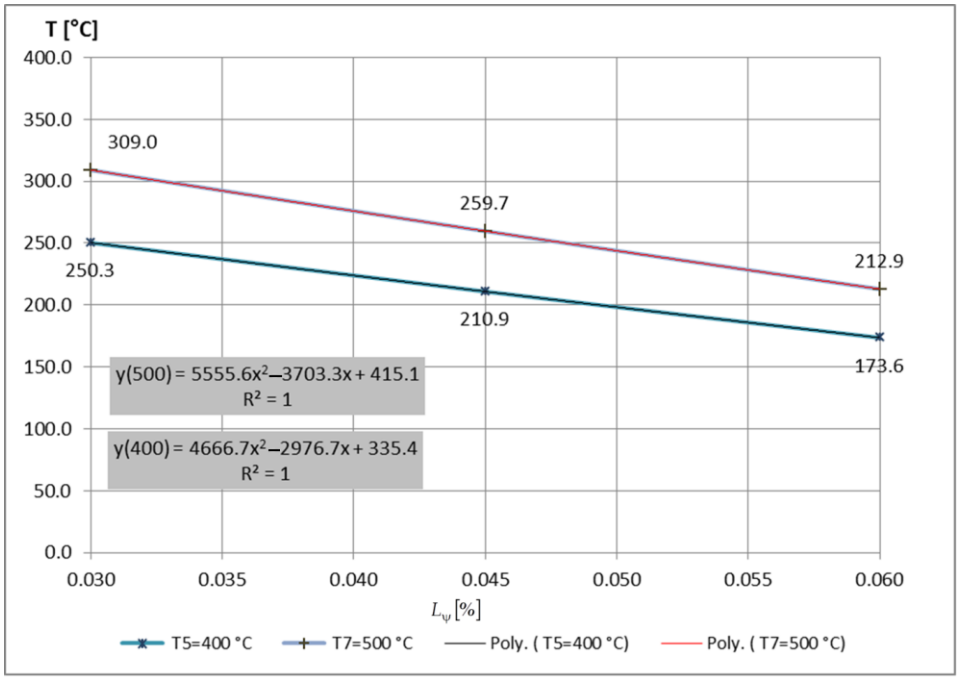

Figure 32. Variation of temperatures along the painted pole, made at a scale of 1:10, on the second interval in Figure 30.

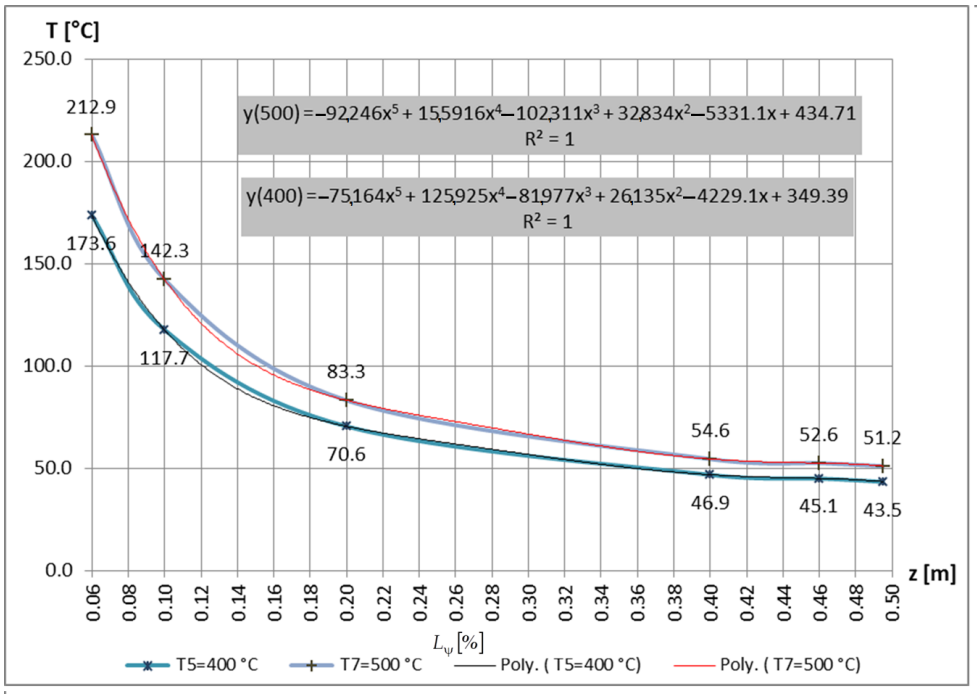

Figure 33. Variation of temperatures along the painted pole, made on a scale of 1:10, on the third interval in Figure 30.

If we switch to the use of dimensionless curves $T_\psi - L_\psi$, then it will be possible to highlight the net advantage of this new approach, because curves with very similar, practically identical slopes will be obtained, which will allow the form of templates or nomograms intended for preliminary calculations to be used in in further research. The explanation could also consist in the fact that differences of the order of a few tens of degrees will not lead to significant deviations of these curves (since we are talking about

percentages of temperatures in the order of hundreds of degrees), even if their nominal temperatures are different.

Next, the authors illustrate the efficiency and net advantage of this new dimensionless approach.

Thus, in Figures 34–39, the curves analyzed in Figures 13–18 are reproduced, but in dimensionless representation.

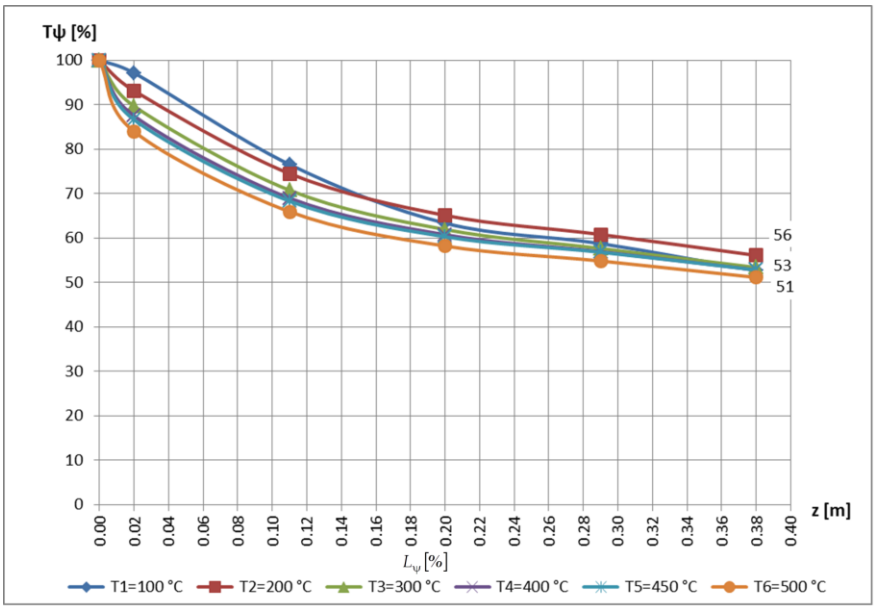

Figure 34. Variation of temperatures along the unpainted prototype, in dimensionless representation.

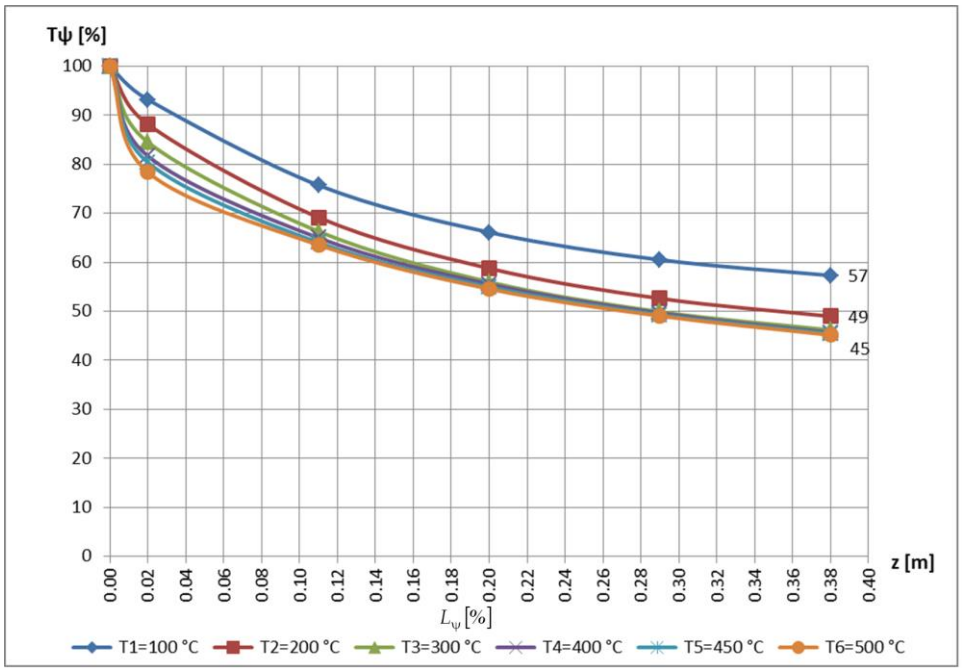

Figure 35. Variation of temperatures along the painted prototype, in dimensionless representation.

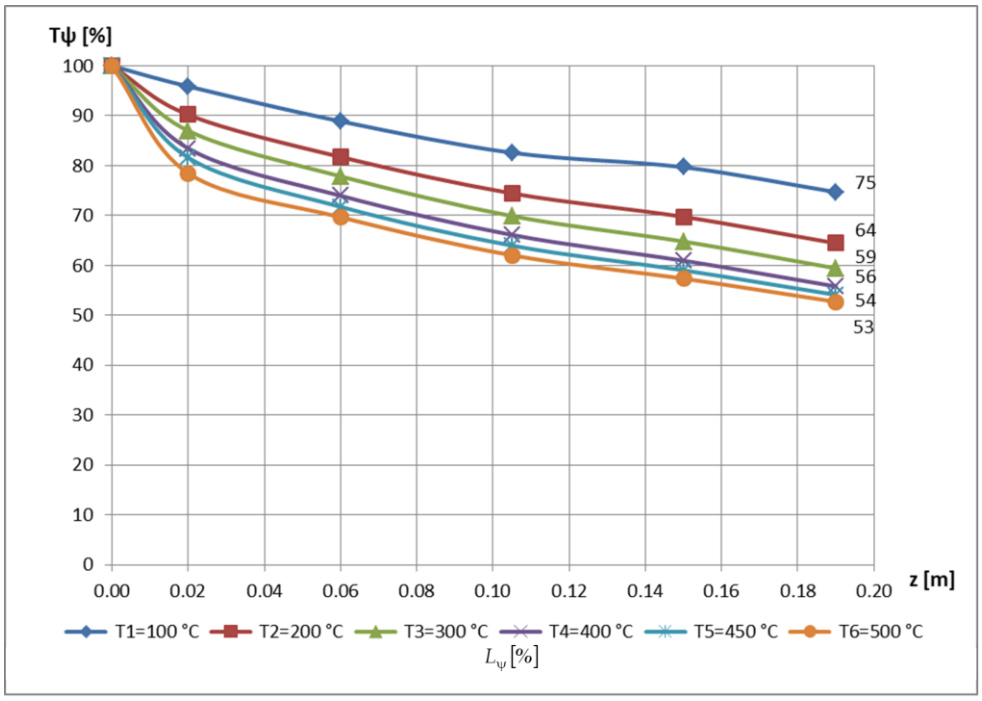

Figure 36. Variation of temperatures along the unpainted 1:2 scale model.

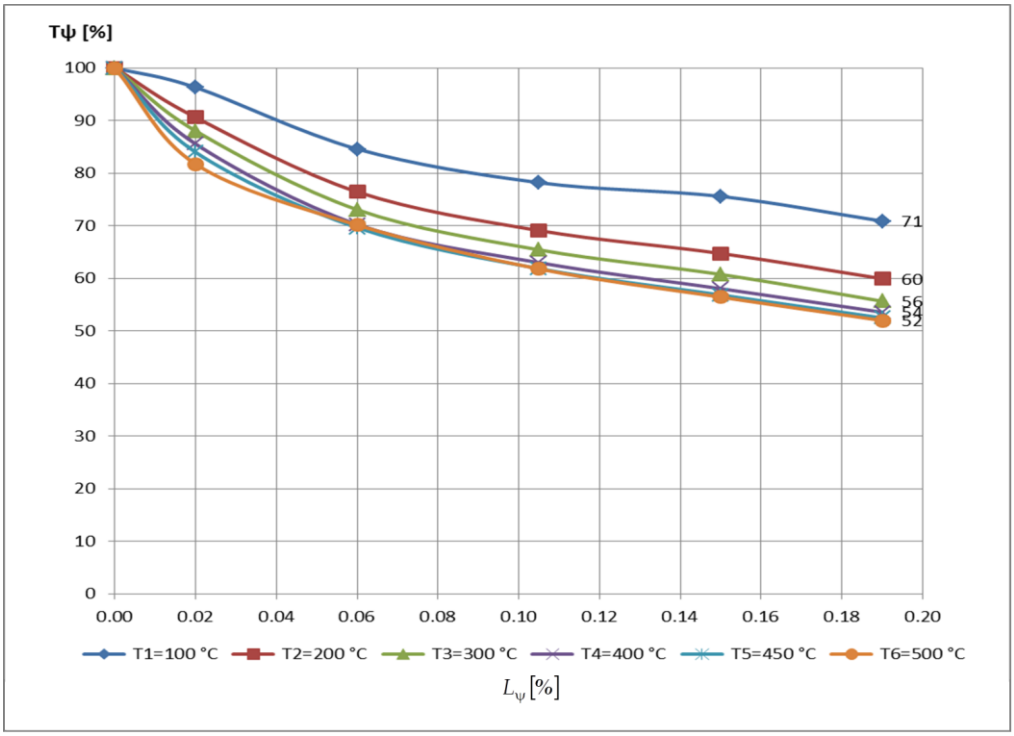

Figure 37. Variation of temperatures along the painted 1:2 scale model.

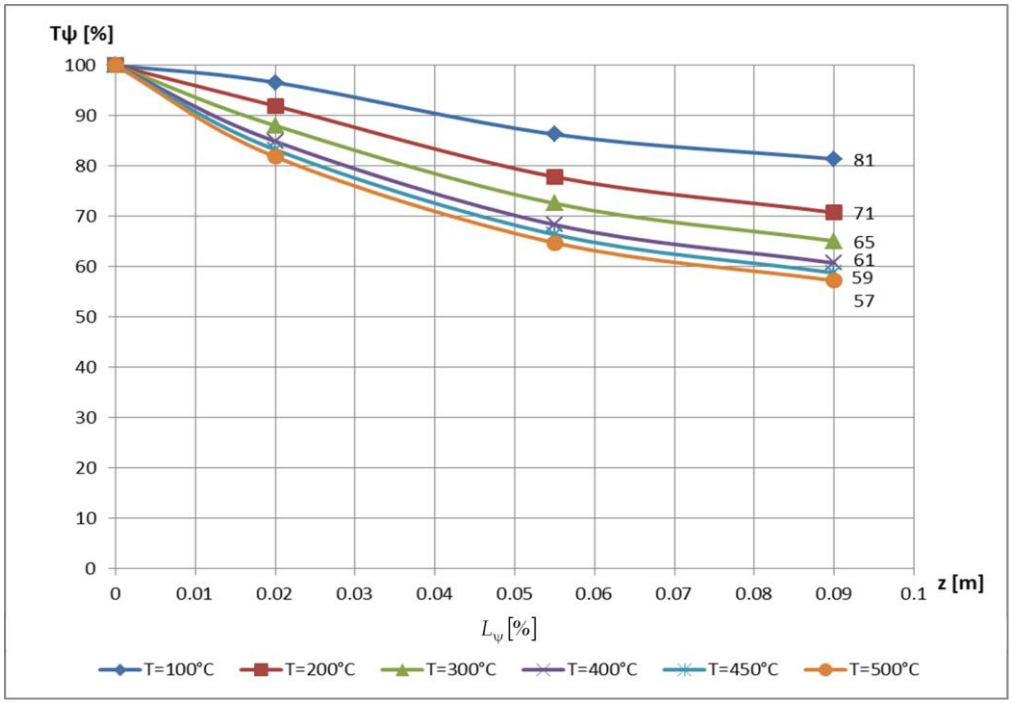

Figure 38. Variation of temperatures along the unpainted 1:4 scale model.

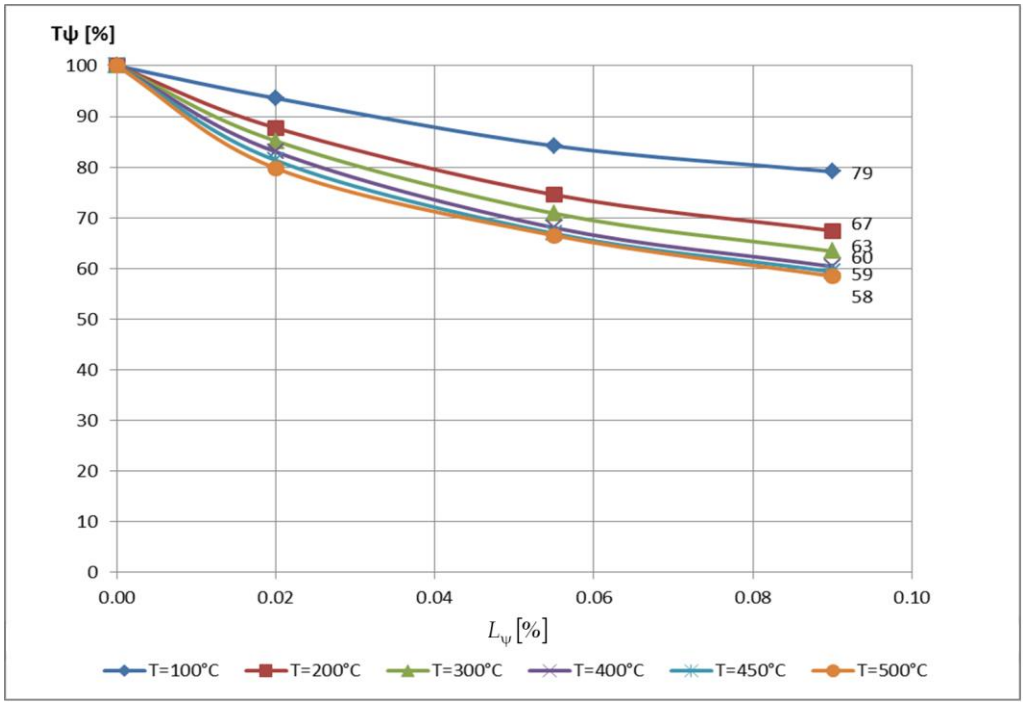

Figure 39. Variation of temperatures along the painted 1:4 scale model.

This very similar behavior of these structural elements, also observable in the above-mentioned figures, justifies the use of a single dimensionless curve $T_\psi - L_\psi$, as a weighted average of them, which will be of great use in an evaluation of the behavior of the structures with the help of MDA.

In this way, as mentioned in Section 3, the testing of these structural elements was carried out with the assurance of a thermal similarity, i.e., reaching identical temperatures in the homologous points of the structures. The most important homologous points from a

thermal point of view were the measurement points at the base, near the upper end of the respective structural element.

In this new approach, those reported in Figures 24 and 25 will take the forms shown in Figures 40 and 41, respectively.

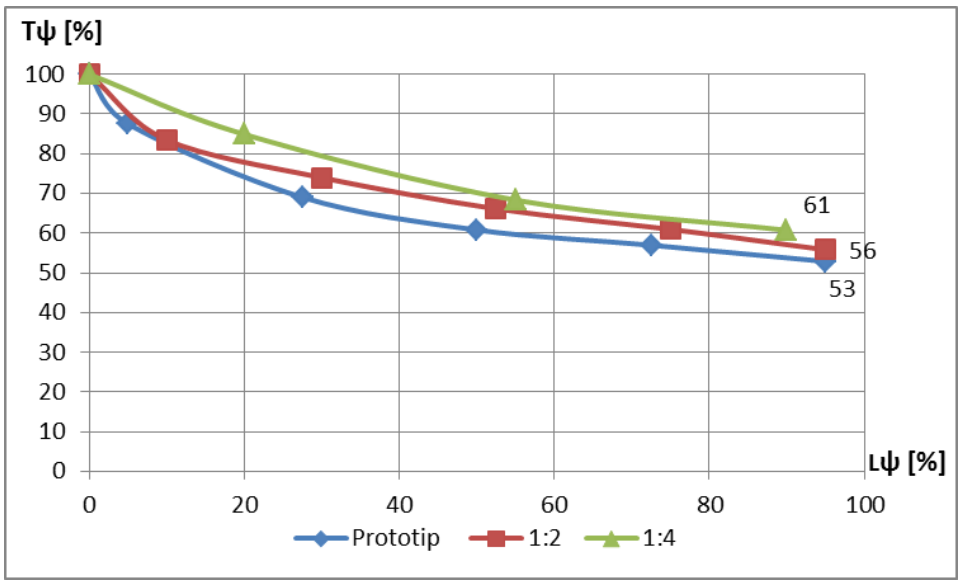

Figure 40. The three segments of unpainted pillars, at 400 °C, in dimensionless coordinate system.

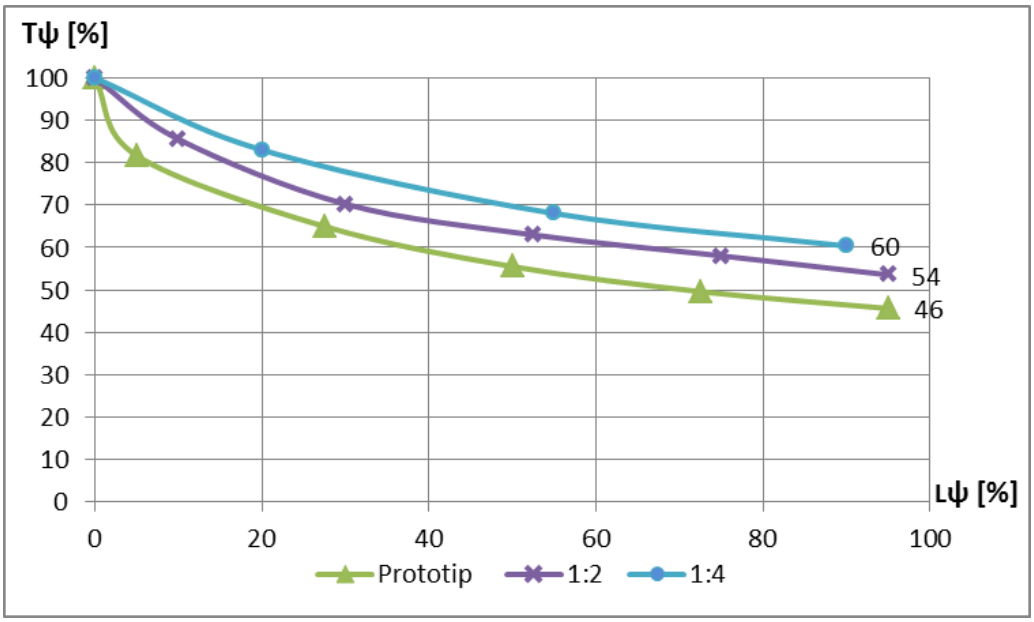

Figure 41. The three segments of painted pillars, at 400 °C, in dimensionless coordinate system.

Similarly, for the pillar made on a scale of 1:10, the diagrams in Figures 26 and 27 will take on the shapes shown in Figures 42 and 43, respectively.

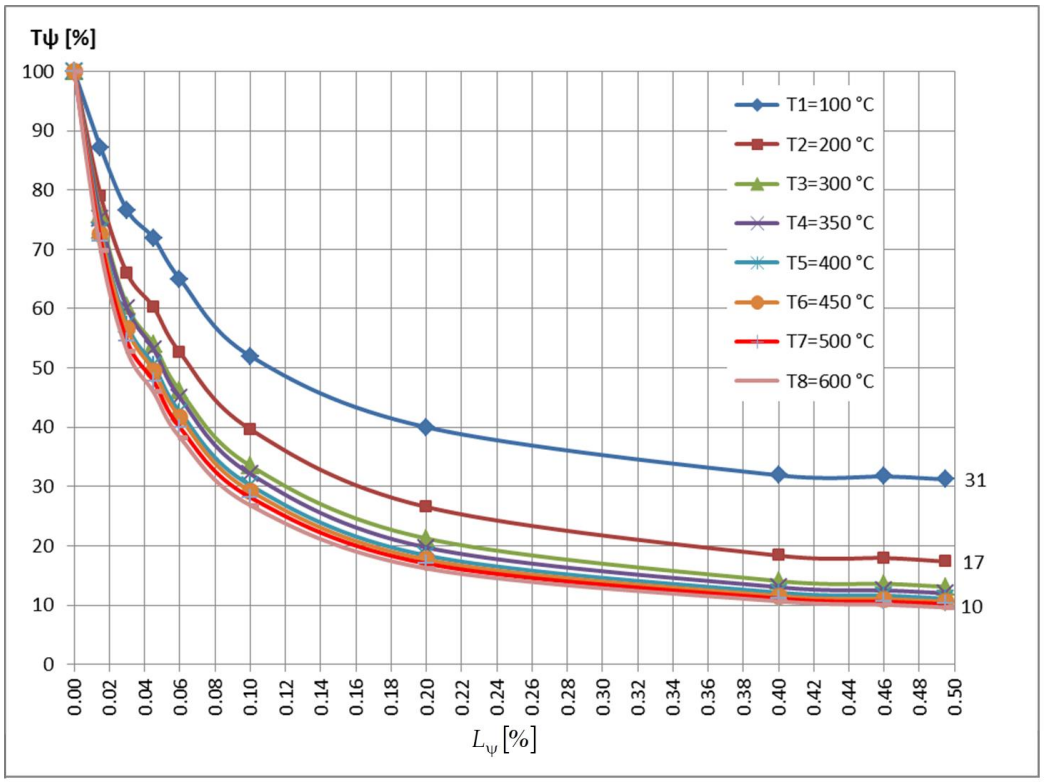

Figure 42. Variation of temperatures along the unpainted pole, in dimensionless representation.

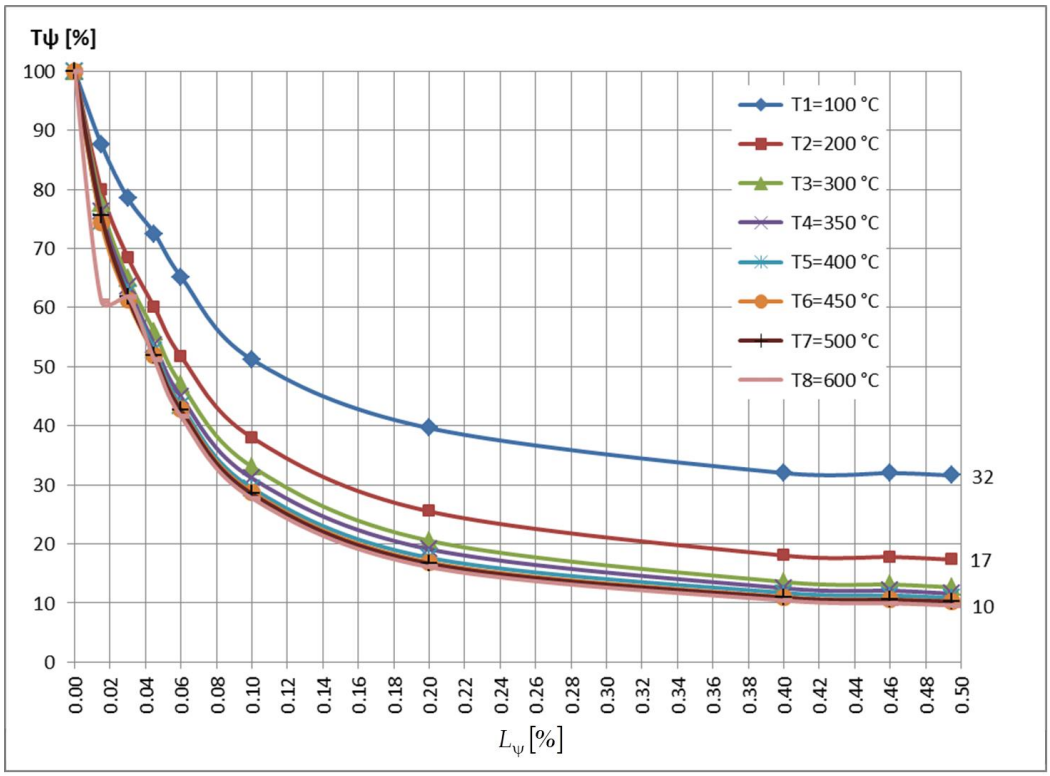

Figure 43. Temperature variation along the painted pole, in dimensionless representation.

It can be observed that, even if the thermal responses of the structural element are reproduced at eight nominal temperatures, starting from $t_{0,nom} = 300\ ^\circ$C, practically all the curves will overlap, which justifies the idea of using a single dimensionless curve $T_\psi - L_\psi$,

as a weighted average of them; the polynomial function, which will approximate it, will serve to perform subsequent calculations.

Obviously, further dividing this representative curve into three subdivisions will give the researcher the possibility of a much more accurate polynomial approximation.

Once this global curve, or even the individual dimensionless curves $T_\psi - L_\psi$ are obtained, the strategy for determining the value of the "m" parameter and its variation law along the structural element $m(z)$ becomes unitary and particularly efficient; in the paper [71] this new approach is detailed.

5. Conclusions

Both the original electrical stand and the results of the investigations carried out with its help were presented, in order to monitor the behavior of a real structural element (a pillar of an existing industrial hall), as well as of some models attached to it, made at different scales (1:2; 1:4; 1:10), all followed in the stabilized thermal regimes. These results were materialized in a series of temperature variation diagrams along the respective structural elements.

Based on these diagrams, the authors went on to illustrate the new approach to diagram analysis, using some normalization steps, gradually moving to dimensionless curves and replacing those resulting from experimental measurements with approximation curves (made using the "curve-fitting" method).

The thermoprotective layer, used in engineering applications, represented a shield in front of the heat flow and prevented the transfer of heat between the structure and the surrounding environment.

The authors express their hope that this new approach, with the help of dimensionless curves $T_\psi - L_\psi$, due to its simplicity and efficiency argued in this article, will be implemented as soon as possible in the thermal study of structural elements subjected to fires by specialists in the field.

The obtained results support the methodology studied by the authors considering the application of MDA to hit transfer phenomena. In this way, measurements made on a scale model, which can be studied in the laboratory, allow quick conclusions to be drawn regarding the behavior of the real model.

In this sense, either the individual curves $T_\psi - L_\psi$ or their representative curve, as their weighted average, can be of great use to specialists and can also serve as a starting point in the creation of nomogram-type databases, related to quick preliminary calculations.

The approach of the easier establishment of the "m" parameter along the structural element and the heat transfer coefficient α_n based on it, essential elements in any analysis of the fire resistance of resistance structures, is also not without importance.

Among the goals pursued by the authors in the near future is even the creation of a database, taking into account first the requirements of the domestic industry, but later also of international companies.

Another future objective would be to carry out some numerical simulations, based on the obtained experimental results, that would validate some pertinent numerical models useful to specialists in the field.

Author Contributions: Conceptualization, I.S. and S.V.; methodology, I.S., I.-R.S. and G.T.; software, Z.A. and B.-P.G.; validation, I.S. and S.V.; formal analysis, I.S. and S.V.; investigation, I.S., S.V., I.-R.S., G.T., V.M.M., T.G., Z.A. and B.-P.G.; resources, I.S. and B.-P.G.; data curation, I.-R.S., G.T., V.M.M. and T.G.; writing—original draft preparation, I.S.; writing—review and editing, I.S. and S.V.; visualization, I.S., S.V., I.-R.S., G.T., V.M.M., T.G., Z.A. and B.-P.G.; supervision, I.S. and S.V.; project administration, I.S.; funding acquisition, I.S. and S.V. All authors have read and agreed to the published version of the manuscript.

Funding: This research received no external funding. The APC was funded by Transylvania University of Brasov.

Data Availability Statement: Not applicable.

Acknowledgments: The authors express their sincere thanks to the ISI-Sys Company of Kassel, Germany for the loan of the VIC-3D optical system, and to the Correlated Solutions Company, USA for the related software.

Conflicts of Interest: The authors declare no conflict of interest.

References

1. Turzó, G. Temperature distribution along a straight bar sticking out from a heated plane surface and the heat flow transmitted by this bar (I)-Theoretical Approach. *Ann. Fac. Eng. Hunedoara-Int. J. Eng.* **2016**, *14*, 49–53.
2. Turzó, G.; Száva, I.R.; Gálfi, B.P.; Száva, I.; Vlase, S.; Hota, H. Temperature Distribution of the Straigth Bar, fixed into a Heated Plane Surface. *Fire Mater.* **2018**, *42*, 202–212. [CrossRef]
3. Turzó, G.; Száva, I.R.; Dancsó, S.; Száva, I.; Vlase, S.; Munteanu, V.; Gălățanu, T.; Asztalos, Z. A New Approach in Heat Transfer Analysis: Reduced-Scale Straight Bars with Massive and Square-Tubular Cross-Sections. *Mathematics* **2022**, *10*, 3680. [CrossRef]
4. Baker, W.; Westine, P.S.; Dodge, F.T. *Similarity Methods in Engineering Dynamics*; Elsevier: Amsterdam, The Netherlands, 1991.
5. Barenblatt, G.I. *Dimensional Analysis*; Gordon and Breach: New York, NY, USA, 1987.
6. Barr, D.I.H. Consolidation of Basics of Dimensional Analysis. *J. Eng. Mech.-ASCE* **1984**, *110*, 1357–1376. [CrossRef]
7. Bejan, A. *Convection Heat Transfer*; John Wiley & Sons: Hoboken, NJ, USA, 2013.
8. Bhaskar, R.; Nigam, A. Qualitative Physics using Dimensional Analysis. *Artif. Intell.* **1990**, *45*, 73–111. [CrossRef]
9. Bridgeman, P.W. *Dimensional Analysis*; Yale University Press: New Haven, CT, USA, 1922; (Reissued in paperbound in 1963).
10. Buckingham, E. On Physically Similar Systems. *Phys. Rev.* **1914**, *4*, 345. [CrossRef]
11. Canagaratna, S.G. Is dimensional analysis the best we have to offer. *J. Chem. Educ.* **1993**, *70*, 40–43. [CrossRef]
12. Carabogdan, G.I.; Badea, A.; Brătianu, C.; Muşatescu, V. *Methods of Analysis of Thermal Energy Processes and Systems*; Technical Publishing House: Bucharest, Romania, 1989. (In Romanian)
13. Carinena, J.F.; Santander, M. Dimensional Analysis. *Adv. Electron. Electron Phys.* **1988**, *72*, 181–258.
14. Carlson, D.E. Some New Results in Dimensional Analysis. *Arch. Ration. Mech. Anal.* **1978**, *68*, 191–210. [CrossRef]
15. Carslaw, H.S.; Jaeger, J.C. *Conduction of Heat in Solid*, 2nd ed.; Oxford Science Publications: New York, NY, USA, 1986.
16. Chen, W.K. Algebraic Theory of Dimensional Analysis. *J. Frankl. Inst.* **1971**, *292*, 403–409. [CrossRef]
17. Coyle, R.G.; Ballicolay, B. Concepts and Software for Dimensional Analysis in Modelling. *IEEE Trans. Syst. Man Cybern.* **1984**, *14*, 478–487. [CrossRef]
18. Fourier, J. *Theorie Analytique de la Chaleur*; Firmin Didot: Paris, France, 1822. (In French)
19. Gibbings, J.C. Dimensional Analysis. *J. Phys. A-Math. Gen.* **1980**, *13*, 75–89. [CrossRef]
20. Gibbings, J.C. A Logic of Dimensional Analysis. *J. Phys. A-Math. Gen.* **1982**, *15*, 1991–2002. [CrossRef]
21. Incropera, F.P.; DeWitt, D.P.; Bergman, T.L.; Lavine, A.S. *Fundamentals of Heat and Mass Transfer*; John Wiley & Sons Ltd.: Chichester, UK, 2002.
22. Jofre, L.; del Rosario, Z.R.; Iaccarino, G. Data-driven dimensional analysis of heat transfer in irradiated particle-laden turbulent flow. *Int. J. Multiph. Flow* **2020**, *125*, 103198. [CrossRef]
23. Környey, T. *Heat Transfer*; Műegyetemi Kiadó: Budapest, Hungary, 1999. (In Hungarian)
24. Langhaar, H.L. *Dimensional Analysis and Theory of Models*; John Wiley & Sons Ltd.: New York, NY, USA, 1951.
25. Martins, R.D.A. The Origin of Dimensional Analysis. *J. Frankl. Inst.* **1981**, *311*, 331–337. [CrossRef]
26. Nakla, M. On fluid-to-fluid modeling of film boiling heat transfer using dimensional analysis. *Int. J. Multiph. Flow* **2011**, *37*, 229–234. [CrossRef]
27. Nezhad, A.H.; Shamsoddini, R. Numerical Three-Dimensional Analysis of the Mechanism of Flow and Heat Transfer in a Vortex Tube. *Therm. Sci.* **2009**, *13*, 183–196. [CrossRef]
28. Pankhurst, R.C. *Dimensional Analysis and Scale Factor*; Chapman & Hall Ltd.: London, UK, 1964.
29. Quintier, G.J. *Fundamentals of Fire Phenomena*; John Wiley & Sons: New York, NY, USA, 2006.
30. Remillard, W.J. Applying Dimensional Analysis. *Am. J. Phys.* **1983**, *51*, 137–140. [CrossRef]
31. Romberg, G. Contribution to Dimensional Analysis. *Inginieur Arch.* **1985**, *55*, 401–412. [CrossRef]
32. Schnittger, J.R. Dimensional Analysis in Design. Journal of Vibration, Accoustic. *Stress Reliab. Des.-Trans. ASME* **1988**, *110*, 401–407. [CrossRef]
33. Sedov, I.L. *Similarity and Dimensional Methods in Mechanics*; MIR Publisher: Moscow, Russia, 1982.
34. de Silva, V.P. Determination of the temperature of thermally unprotected steel members under fire situations considerations on the section factor. *Lat. Am. J. Solids Struct.* **2006**, *3*, 113–125.
35. Szekeres, P. Mathematical Foundations of Dimensional Analysis and the Question of Fundamental Units. *Int. J. Theor. Phys.* **1978**, *17*, 957–974. [CrossRef]
36. Șova, M.; Șova, D. *Thermotechnics*; Transilvania University Press: Brașov, Romania, 2001; Volume II.
37. Șova, D. *Heat Engineering*; Transilvania University Press: Brasov, Romania, 2006; ISBN 9789736357664.
38. Șova, D. *Applied Thermodynamics*; Transilvania University Press: Brasov, Romania, 2015; ISBN 9786061907144.
39. Ştefănescu, D.; Marinescu, M.; Dănescu, A. *Heat Transfer in Technique*; Tehnică: Bucureşti, Romania, 1982; Volume I.
40. VDI. *VDI-Wärmeatlas*, 7th ed.; Verein Deutscher Ingenieure: Düsseldorf, Germany, 1994.

41. Zierep, J. *Similarity Laws and Modelling*; Marcel Dekker: New York, NY, USA, 1971.
42. Aglan, A.A.; Redwood, R.G. Strain-Hardening Analysis of Beams with 2 WEB- Rectangular Holes. *Arab. J. Sci. Eng.* **1987**, *12*, 37–45.
43. Al-Homoud, M.S. Performance characteristics and practical applications of common building thermal insulation materials. *Build. Environ.* **2005**, *40*, 353–366. [CrossRef]
44. Bączkiewicz, J.; Malaska, M.; Pajunen, S.; Heinisuo, M. Experimental and numerical study on temperature distribution of square hollow section joints. *J. Constr. Steel Res.* **2018**, *142*, 31–43. [CrossRef]
45. Bailey, C. Indicative fire tests to investigate the behaviour of cellular beams protected with intumescent coatings. *Fire Saf. J.* **2004**, *39*, 689–709. [CrossRef]
46. Ferraz, G.; Santiago, A.; Rodrigues, J.P.; Barata, P. Thermal Analysis of Hollow Steel Columns Exposed to Localized Fires. *Fire Technol.* **2016**, *52*, 663–681. [CrossRef]
47. Franssen, J.-M. Calculation of temperature in fire-exposed bare steel structures: Comparison between ENV 1993-1-2 and EN 1993-1-2. *Fire Saf. J.* **2006**, *41*, 139–143. [CrossRef]
48. Franssen, J.-M.; Real, P.V. *Fire Design of Steel Structures, ECCS Eurocode Design Manuals, ECCS-European Convention for Constructional Steelwork*; Ernst & Sohn: Berlin, Germany, 2010.
49. Gao, F.; Guan, X.-Q.; Zhu, H.P.; Liu, X.-N. Fire resistance behaviour of tubular T-joints reinforced with collar plates. *J. Constr. Steel Res.* **2015**, *115*, 106–120. [CrossRef]
50. Ghojel, J.I.; Wong, M.B. Heat transfer model for unprotected steel members in a standard compartment fire with participating medium. *J. Constr. Steel Res.* **2005**, *61*, 825–833. [CrossRef]
51. Xiao, B.Q.; Li, Y.P.; Long, G.B. A Fractal Model of Power-Law Fluid through Charged Fibrous Porous Media by using the Fractional-Derivative Theory. *FRACTALS- Complex Geom. Patterns Scaling Nat. Soc.* **2022**, *30*, 2250072. [CrossRef]
52. Xiao, B.Q.; Fang, J.; Long, G.B.; Tao, Y.Z.; Huang, Z.J. Analysis of Thermal Conductivity of Damaged Tree-Like Bifurcation Network with Fractal Roughened Surfaces. *FRACTALS-Complex Geom. Patterns Scaling Nat. Soc.* **2022**, *30*, 2250104. [CrossRef]
53. Long, G.; Liu, Y.; Xu, W.; Zhou, P.; Zhou, J.; Xu, G.; Xiao, B. Analysis of Crack Problems in Multilayered Elastic Medium by a Consecutive Stiffness Method. *Mathematics* **2022**, *10*, 4403. [CrossRef]
54. Kado, B.; Mohammad, S.; Lee, Y.H.; Shek, P.N.; Ab Kadir, M.A. Temperature Analysis of Steel Hollow Column Exposed to Standard Fire. *J. Struct. Technol.* **2018**, *3*, 1–8.
55. Khan, M.A.; Shah, I.A.; Rizvi, Z.; Ahmad, J. A numerical study on the validation of thermal formulations towards the behaviours of RC beams. *Sci. Mater. Today Proc.* **2019**, *17*, 227–234. [CrossRef]
56. Krishnamoorthy, R.R.; Bailey, C.G. Temperature distribution of intumescent coated steel framed connection at elevated temperature. In Proceedings of the Nordic Steel Construction Conference '09, Malmo, Sweden, 2–4 September 2009; Swedish Institute of Steel Construction: Stockholm, Sweden, 2009; Publication 181, Volume I, pp. 572–579.
57. Lawson, R.M. Fire engineering design of steel and composite Buildings. *J. Constr. Steel Res.* **2001**, *57*, 1233–1247. [CrossRef]
58. Levac, M.L.J.; Soliman, H.M.; Ormiston, S.J. Three-dimensional analysis of fluid flow and heat transfer in single- and two-layered micro-channel heat sinks. *Heat Mass Transf.* **2011**, *47*, 1375–1383. [CrossRef]
59. Noack, J.; Rolfes, R.; Tessmer, J. New layerwise theories and finite elements for efficient thermal analysis of hybrid structures. *Comput. Struct.* **2003**, *81*, 2525–2538. [CrossRef]
60. Papadopoulos, A.M. State of the art in thermal insulation materials and aims for future developments. *Energy Build.* **2005**, *37*, 77–86. [CrossRef]
61. Tafreshi, A.M.; Di Marzo, M. Foams and gels as temperature protection agents. *Fire Saf. J.* **1999**, *33*, 295–305. [CrossRef]
62. Yang, K.-C.; Chen, S.J.; Lin, C.-C.; Lee, H.-H. Experimental study on local buckling of fire-resisting steel columns under fire load. *J. Constr. Steel Res.* **2005**, *61*, 553–565. [CrossRef]
63. Yang, J.; Shao, Y.B.; Chen, C. Experimental study on fire resistance of square hollow section (SHS) tubular T-joint under axial compression. *Adv. Steel Constr.* **2014**, *10*, 72–84.
64. Wong, M.B.; Ghojel, J.I. Sensitivity analysis of heat transfer formulations for insulated structural steel components Fire. *Saf. J.* **2003**, *38*, 187–201. [CrossRef]
65. Vlase, S.; Teodorescu-Draghicescu, H.; Calin, M.R.; Scutaru, M.L. Advanced Polylite composite laminate material behavior to tensile stress on weft direction. *J. Optoelectron. Adv. Mater.* **2022**, *14*, 658–663.
66. Alshqirate, A.A.Z.S.; Tarawneh, M.; Hammad, M. Dimensional Analysis and Empirical Correlations for Heat Transfer and Pressure Drop in Condensation and Evaporation Processes of Flow Inside Micropipes: Case Study with Carbon Dioxide (CO_2). *J. Braz. Soc. Mech. Sci. Eng.* **2012**, *34*, 89–96.
67. Andreozzi, A.; Bianco, N.; Musto, M.; Rotondo, G. Scaled models in the analysis of fire-structure interaction. In Proceedings of the 33rd UIT (Italian Union of Thermo-Fluid-Dynamics) Heat Transfer Conference, L'Aquila, Italy, 22–24 June 2015; IOP: Bristol, UK, 2015; Volume 655, p. 012053. [CrossRef]
68. He, S.-B.; Shao, Y.-B.; Zhang, H.-Y.; Wang, Q. Parametric study on performance of circular tubular K-joints at elevated temperature. *Fire Saf. J.* **2015**, *71*, 174–186. [CrossRef]
69. Illan, F.; Viedma, A. Experimental study on pressure drop and heat transfer in pipelines for brine based ice slurry Part II: Dimensional analysis and rheological Model. *Int. J. Refrig.-Rev. Int. Du Froid* **2009**, *32*, 1024–1031. [CrossRef]

70. Gálfi, B.-P.; Száva, I.; Șova, D.; Vlase, S. Thermal Scaling of Transient Heat Transfer in a Round Cladded Rod with Modern Dimensional Analysis. *Mathematics* **2021**, *9*, 1875. [CrossRef]
71. Munteanu (Száva), I.R. Investigation Concerning Temperature Field Propagation along Reduced Scale Modelled Metal Structures. Ph.D. Thesis, Transilvania University of Brasov, Brasov, Romania, 2018.
72. Száva, I.R.; Șova, D.; Dani, P.; Élesztős, P.; Száva, I.; Vlase, S. Experimental Validation of Model Heat Transfer in Rectangular Hole Beams Using Modern Dimensional Analysis. *Mathematics* **2022**, *10*, 409. [CrossRef]
73. Șova, D.; Száva, I.R.; Jármai, K.; Száva, I.; Vlase, S. Modern method to analyze the Heat Transfer in a Symmetric Metallic Beam with Hole. *Symmetry* **2022**, *14*, 769. [CrossRef]
74. Trif, I.; Asztalos, Z.; Kiss, I.; Élesztős, P.; Száva, I.; Popa, G. Implementation of the Modern Dimensional Analysis in Engineering Problems; Basic Theoretical Layouts. *Ann. Fac. Eng. Hunedoara* **2019**, *17*, 73–76.
75. Szirtes, T. The Fine Art of Modelling. *SPAR J. Eng. Technol.* **1992**, *1*, 37.
76. Szirtes, T. *Applied Dimensional Analysis and Modelling*; McGraw-Hill: Toronto, ON, Canada, 1998.
77. Száva, I.; Szirtes, T.; Dani, P. An Application of Dimensional Model Theory in the Determination of the Deformation of a Structure. *Eng. Mech.* **2006**, *13*, 31–39.
78. Száva, R.I.; Száva, I.; Vlase, S.; Gálfi, P.B.; Jármai, K.; Gălățanu, T.; Popa, G.; Asztalos, Z. Modern Dimensional Analysis-Based Steel Column' Heat Transfer Evaluation using Multiple Experiments. *Symmetry* **2022**, *14*, 1952. [CrossRef]
79. Dani, P.; Száva, I.R.; Kiss, I.; Száva, I.; Popa, G. Principle Schema of an Original Full-, and Reduced-Scale Testing Bench, Destined to Fire Protection Investigations. *Ann. Fac. Eng. Hunedoara-Int. J. Eng.* **2018**, *16*, 149–152.
80. Gálfi, B.P.; Száva, R.I.; Száva, I.; Vlase, S.; Gălățanu, T.; Jármai, K.; Asztalos, Z.; Popa, G. Modern Dimensional Analysis based on Fire-Protected Steel Members' Analysis using Multiple Experiments. *Fire* **2022**, *5*, 210. [CrossRef]